Evolutionary loss of foot muscle during development with characteristics of atrophy and no evidence of cell death

Mai P. Tran[1], Rio Tsutsumi[1], Joel M. Erberich[1], Kevin D. Chen[1], Michelle D. Flores[1], and Kimberly L. Cooper[1,*]

[1]Division of Biological Sciences, Section of Cellular and Developmental Biology, University of California San Diego, La Jolla, California 92093, USA.

[*]For correspondence: kcooper@ucsd.edu

Abstract

Many species that run or leap across sparsely vegetated habitats, including horses and deer, evolved the severe reduction or complete loss of foot muscles as skeletal elements elongated and digits were lost, and yet the developmental mechanisms remain unknown. Here, we report the natural loss of foot muscles in the bipedal jerboa, *Jaculus jaculus*. Although adults have no muscles in their feet, newborn animals have muscles that rapidly disappear soon after birth. We were surprised to find no evidence of apoptotic or necrotic cell death during stages of peak myofiber loss, countering well-supported assumptions of developmental tissue remodeling. We instead see hallmarks of muscle atrophy, including an ordered disassembly of the sarcomere associated with upregulation of the E3 ubiquitin ligases, *MuRF1* and *Atrogin-1*. We propose that the natural loss of muscle, which remodeled foot anatomy during evolution and development, involves cellular mechanisms that are typically associated with disease or injury.

Introduction

Muscles in the feet of birds, reptiles, and mammals were lost multiple times in the course of limb evolution, usually coinciding with the loss of associated digits and elongation of remaining skeletal elements (Hudson, 1937; Raikow, 1987; Pavaux and Lignereux, 1995; Botelho et al., 2014; Abdala et al., 2015; Berman, 1985; Cunningham, 1883; Souza et al., 2010). Despite its frequent occurrence, the developmental mechanisms that lead to the natural absence of adult limb muscle are not known. We focus here on a representative example of distal limb muscle loss in the bipedal three-toed jerboa (*Jaculus jaculus*), a small laboratory rodent model for evolutionary developmental biology, to determine if evolutionary muscle loss conforms to expectations based on what was previously known about muscle cell biology.

The hindlimb architecture of the adult jerboa is strikingly similar by convergence to the more familiar hooved animals, like horses and deer, including the disproportionately elongated

foot that lacks all intrinsic muscle (Berman, 1985; Cunningham, 1883). The tendons were retained and expanded in each of the anatomical positions where flexor muscles are absent (Figure 1A,B and Figure1 – figure supplement 1A,B) and serve to resist hyperextension when the terminal phalanx contacts the ground during locomotion (Lochner et al., 1980; Moore et al., 2017). The evolutionary origin of jerboa intrinsic foot muscle loss lies deep in the phylogenetic tree of Dipodoid rodents. Compared to the ancestral state, the number of intrinsic foot muscles are reduced from sixteen to six in pygmy jerboas (Stein, 1990) which diverged from the three-toed jerboa lineage more than 20 million years ago (Wu et al., 2012; Pisano et al., 2015).

The mechanisms of limb muscle development have been extensively studied in traditional model systems, and its degeneration has been studied after injury and during disease. Briefly, limb muscle progenitors are specified from mesodermal cells at the ventrolateral edge of the dermomyotome in somites aligned with the prospective limb. These cells delaminate and migrate into the limb bud as dorsal and ventral muscle masses that proliferate and initiate a myoblast specification program (Chevallier et al., 1977; Christ et al., 1977; Hayashi and Ozawa, 1991; Murphy and Kardon, 2011). The muscle masses are then subdivided into individual muscle groups in response to cues from the developing muscle connective tissue, which is derived from limb field lateral plate mesoderm (Hayashi and Ozawa, 1991; Kardon, 1998; Kardon et al., 2003; Wortham, 1948). They then initiate a differentiation program, which includes cell fusion to form aligned multinucleated myofibers (Abmayr and Pavlath, 2012; Kelly and Zacks, 1969).

Each differentiated myofiber produces an assemblage of Z-body proteins, Actin filaments, and non-muscle Myosin that form premyofibrils (Ono, 2010; Rhee et al., 1994; Sanger and Sanger, 2008; Sanger et al., 2002). Desmin, α-Actinin, and the Z-body portion of Titin also begin to organize (Furst et al., 1989; Sanger et al., 2002). Subsequent uncoiling of Titin increases Z-body spacing, and integration of embryonic skeletal muscle Myosin results in formation of nascent myofibrils (Ono, 2010; Sanger et al., 2010). Further maturation of the nascent myofibril into a mature myofibril involves incorporation of additional proteins that are important for sarcomere structure and function, and Z-lines are aligned and properly spaced to bring sarcomeres into register (Ehler and Gautel, 2008; Sanger et al., 2010). Failure at any point of myoblast specification, migration, myofiber differentiation, or myofibril maturation compromises muscle function and manifests as muscle degenerative disease in humans (Bönnemann and Laing, 2004; Laing and Nowak, 2005; Morita et al., 2005).

Working backward in time from the adult jerboa phenotype, we found that two of the three flexor muscle groups differentiate as multinucleated myofibers that initiate sarcomere

assembly, as in other species. However, almost all jerboa intrinsic foot muscle is lost within a few days shortly after birth. Despite the rapid and near complete loss of myofibers, we found no molecular or ultrastructural evidence of apoptotic or necrotic cell death, no accumulation of autophagic vesicles, and no macrophage infiltration. Instead, we observed evidence of ordered sarcomere disassembly and upregulation of muscle-specific ubiquitin ligases, *MuRF1* and *Atrogin-1*. Although the ultimate fate of intrinsic foot myofibers after loss of muscle identity remains unknown, these data suggest that the mechanism of myofiber loss is similar to atrophy, which is typically considered a pathological response to injury or disease.

Results

The absence of intrinsic foot muscle in the adult jerboa could be due to a failure of early myoblasts to migrate into and/or to differentiate in the distal limb. Alternatively, embryonic muscles may form but not persist through development to the adult. In transverse sections of newborn mouse feet, immunofluorescent detection of skeletal muscle myosin heavy chain reveals each intrinsic muscle group (Figure1 – figure supplement 1G). In newborn jerboas, we observed two of the three groups of flexor muscles. While the *m. lumbricales* never form, the jerboa has a single *m. flexor digitorum brevis* and three pinnate *m. interossei* that are not present in adults (Figure1 – figure supplement 1H).

Postnatal growth of vertebrate skeletal muscle typically involves an increase in myofiber number (hyperplasia) within the first week, followed by an increase in myofiber size (hypertrophy) (Chiakulas and Pauly, 1965; Gokhin et al., 2008; White et al., 2010). In order to understand the dynamics of muscle growth and loss, we quantified the rate of myofiber hyperplasia at two-day intervals after birth of the mouse and jerboa, focusing on the representative interosseous muscle that is associated with the third metatarsal (Figure 1E,F). As expected in the mouse, we observed a steady increase in the average number of myofibers in cross section from birth to P8 (Figure 1C). In contrast, the number of myofibers in the third interosseous of the jerboa foot rapidly declines beginning at approximately P4, and few myofibers remain by P8 (Figure 1D).

It is possible that the rate of myofiber loss outpaces a typical rate of new cell addition such that muscles with the potential to grow are instead steadily diminished. Alternatively, myofiber loss may be accelerated by a compromised ability to form new myofibers and to add nuclei to growing myofibers. To distinguish these hypotheses, we analyzed cohorts of animals two days after intraperitoneal BrdU injection at P0, P2, or P4. Since multinucleated jerboa foot myofibers are postmitotic (Figure 2 - figure supplement 1), we reasoned that BrdU+ nuclei

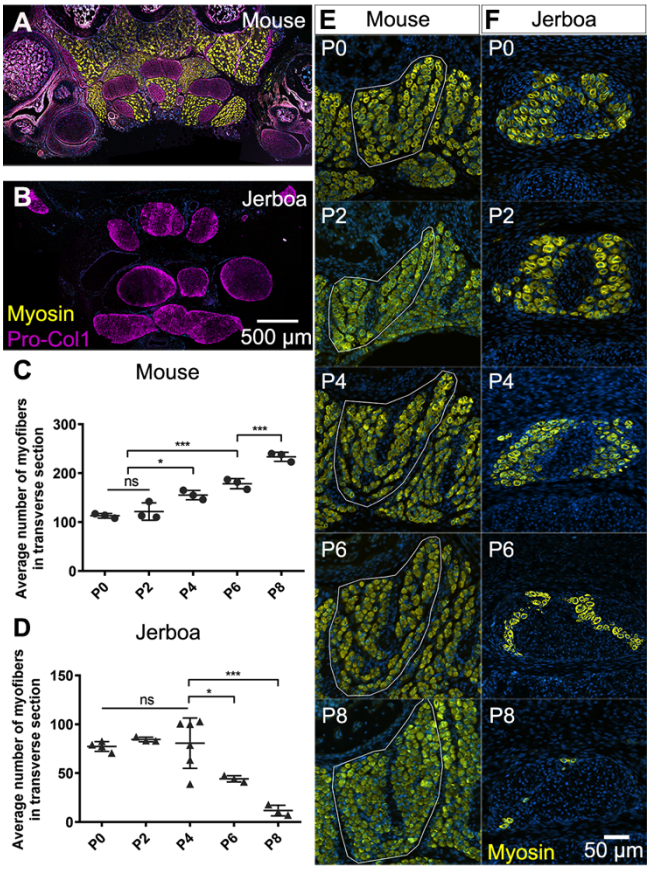

Figure 1: Muscles are rapidly lost in the neonatal jerboa foot.
(A and B) Transverse sections of adult (A) mouse and (B) jerboa foot.
(C and D) Mean and standard deviation of the number of myofibers in transverse sections of third digit interosseous muscle at two-day intervals from birth to postnatal day 8. (C) Mouse P0-P8, n=3 animals each. P0-P4 (p=0.0062), P2-P4 (p=0.0262), P0-P6 (p=0.0002), P2-P6 (p=0.0007), P6-P8 (p=0.0009). (D) Jerboa P0, n=4 animals; P2, P6, P8, n=3 animals each; P4, n=6 animals. P4-P6 (p=0.0376), P4-P8 (p=0.0002).
(*p<0.05, **p<0.01, ***p<0.001)
(E and F) Representative transverse sections of interosseous muscle of the third digit of (E) mouse and (F) jerboa at each stage. For all: top dorsal; bottom ventral.

present within Dystroglycan+ myofiber membranes were added by myocyte fusion during the two-day window after they were labeled as myoblasts or myocytes in S-phase (Figure 2A). When normalized to the total number of myofiber nuclei, we found that myocytes fuse to form multinucleated myofibers in jerboa hand muscle at a consistent rate from P0 to P6. However, their incorporation into jerboa foot muscle decreased significantly after P2 (Figure 2B). These results suggest that myofiber loss, which begins at P4, is preceded by reduced myogenesis.

The reduced rate of myocyte incorporation could be due to reduced numbers of muscle progenitor cells or to an inability of these cells to mature and fuse. To distinguish these possibilities by quantifying proliferative muscle progenitor cells, we analyzed animals two hours after BrdU injection at P0, P2, and P4 and counted the number of BrdU+ nuclei located between the Dystroglycan+ myofiber membrane and the Laminin+ basal lamina (Fig. 2C). Normalized to the total number of myofibers, we found that the number of proliferative progenitor cells in

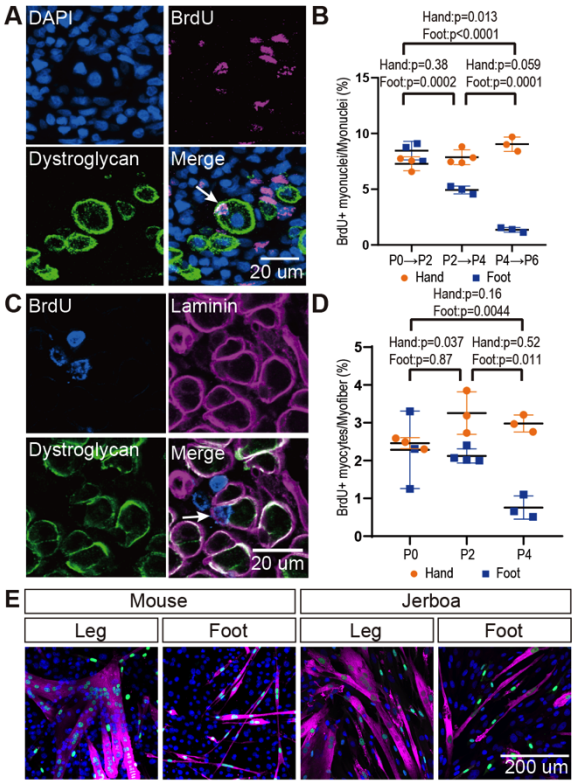

Figure 2: The rate of myocyte fusion is reduced prior to myofiber loss.

(A) Newly fused nuclei within Dystroglycan+ myofiber membranes (arrow) can be distinguished two days after labeling with BrdU.

(B) The mean and standard deviation of BrdU+ myonuclei (putative fusion events) normalized to all myofiber nuclei in sections of jerboa hand and foot muscles at intervals from P0 to P6. Foot at P0-P2, P2-P4, P4-P6, Hand at P0-P2, P4-P6, n=3 animals each. Hands at P2-P4, n=4 animals.

(C) Proliferative muscle progenitor cells that are BrdU+ are found outside Dystroglycan+ membrane and inside the Laminin+ basal lamina (Arrow).

(D) The mean and standard deviation of BrdU+ muscle progenitor cells was normalized to the number of myofibers in sections of jerboa hand and foot muscles at P0, P2, and P4. n=4 animals each.

(E) Differentiated myofibers after 6 days of culturing primary muscle progenitor cells isolated from lower leg and foot muscles of mouse and jerboa. Green, Myogenin; Magenta, Myosin.

jerboa foot muscle significantly decreased from P0 to P4 compared to hand muscles that showed no change over time (Fig. 2D). These results suggest that a reduced number of muscle progenitor cells might contribute to the reduced prevalence of myocyte fusion events.

We next tested whether compromised proliferation and differentiation of jerboa foot muscle progenitors is cell autonomous or non-cell autonomous. We isolated single cells, including myoblasts and myocytes but excluding myofibers, by mechanical trituration and enzymatic digestion of P1 jerboa and mouse lower leg and foot muscles (Danoviz and Yablonka-Reuveni, 2012a). After 6 days and 9 days of culture, we detected Myogenin+ differentiating myocytes and Myosin+ fully differentiated myofibers in primary cell cultures isolated from each muscle (Fig. 2E). We did not detect a significant decline in the number of differentiated cells over time (Figure 2 – figure supplement 2). Jerboa foot muscle cell differentiation and survival *in vitro* days after cell number begins to decline *in vivo* suggests that loss of jerboa foot myofibers is initiated non-cell autonomously.

The rapid and almost complete loss of differentiated myofibers *in vivo* from P4 to P8 suggested these cells die, since individual cells or groups of cells are commonly eliminated by apoptosis during development (Brill et al., 1999; Fernández-Terán et al., 2006). We therefore tested the hypothesis that neonatal intrinsic foot muscles undergo apoptosis by implementing the TUNEL assay to detect DNA fragmentation and by immunofluorescent detection of cleaved Caspase-3, a key protein in the apoptotic program (Elmore, 2007). Each revealed keratinocyte apoptosis in hair follicles, which are known to undergo programmed cell death, as a positive control in the same tissue sections (Magerl et al., 2001). However, TUNEL or cleaved Caspase-3 positive jerboa foot myofibers or cells in their vicinity were an extreme rarity (0.25% of myofibers) in animals ranging from P0 to P8 and comparable to mouse myofibers suggesting muscle is not eliminated by apoptosis (Figure 3A,B and Figure 3 – figure supplement 1).

Alternatively, myofiber loss may occur through a cell death mechanism that is first characterized by plasma membrane permeability, such as necrosis (Berghe et al., 2014). To test this hypothesis, we injected Evans blue dye (EBD), a fluorescent molecule that accumulates in cells with compromised plasma membranes (Hamer et al., 2002; Matsuda et al., 1995), into the peritoneum of P3 and P4 neonatal jerboas 24 hours before euthanasia. Although we detected EBD in mechanically injured myofibers of the gastrocnemius as a control, we saw no EBD fluorescence in jerboa foot myofibers or in surrounding cells (Figure 3C and Figure 3 – figure supplement 2). We also saw no Annexin V immunofluorescence on the surface of jerboa foot myofibers, another hallmark of dying cells that flip Annexin V to the outer plasma membrane (Figure 3D and Figure 3 – figure supplement 2).

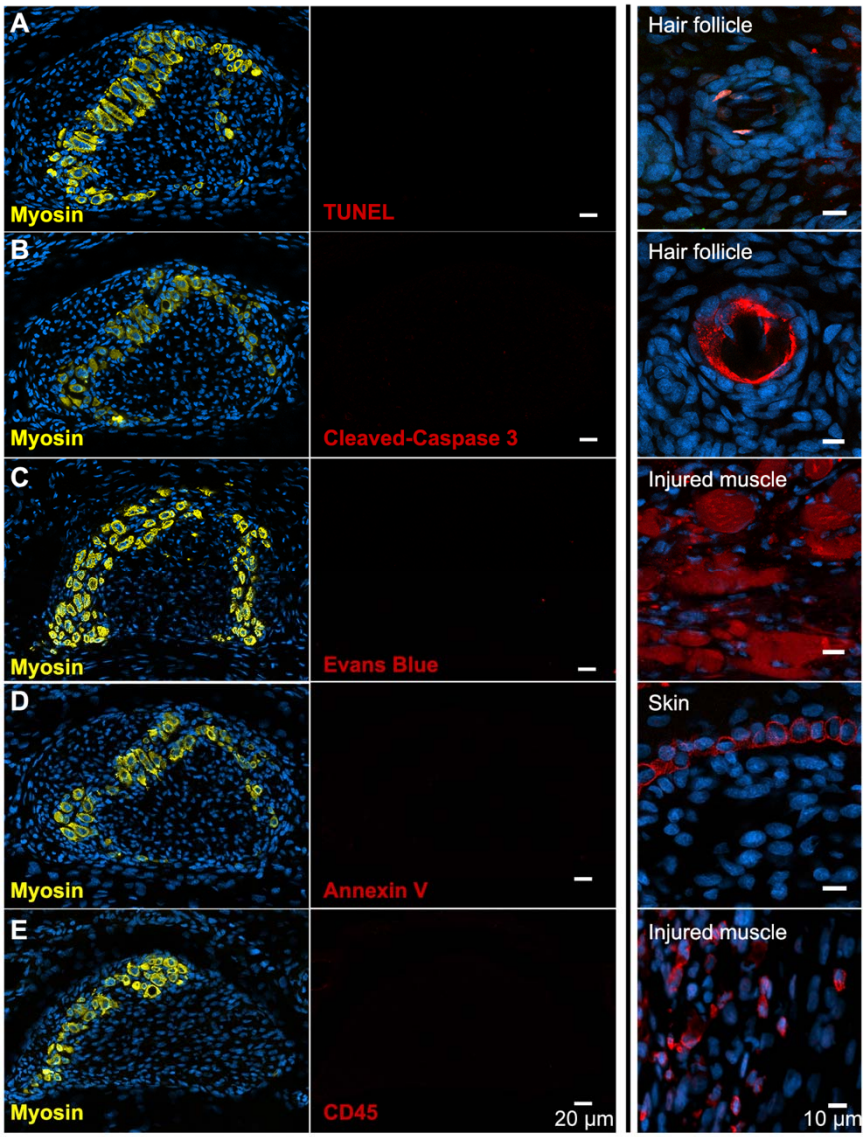

Figure 3: There is no evidence of apoptosis, necrosis, or macrophage infiltration.

(A and B) TUNEL and cleaved Caspase-3 staining for apoptotic nuclei in transverse sections of third digit interosseous muscle in the P6 jerboa foot and of positive control (TUNEL, n=3 animals; cleaved Caspase-3, n=2 animals). See also Figure 3 – figure supplement 1 for more stages.

(C) EBD detection in transverse section of third digit interosseous muscle in the P5 jerboa foot and of positive control (n=5 animals). See also Figure 3 – figure supplement 2 for more stages.

(D) Annexin V immunofluorescence in longitudinal section of third digit interosseous muscle in the P6 jerboa foot and of positive control (n=3 animals). See also Figure 3 – figure supplement 2 for more stages.

(E) CD45 immunofluorescence in transverse section of third digit interosseous muscle in the P6 jerboa foot and of positive control (n=3 animals). See also Figure 3 – figure supplement 3 for more stages and for an additional macrophage marker, F4/80.

Since we observed no direct evidence of cell death, we asked whether there was an immune response that might be an indirect proxy for undetected death. Dying muscle cells frequently recruit phagocytic macrophages that engulf cellular debris (Arnold et al., 2007; Londhe and Guttridge, 2015; Tidball and Wehling-Henricks, 2007). We predicted that myofibers that die by any mechanism that produces cellular debris might recruit macrophages that are detectable by expression of the F4/80 glycoprotein. However, consistent with the lack of evidence of cell death in the jerboa foot, no F4/80^{+} macrophages were found among myofibers from birth to P7 (Figure 3 – figure supplement 3). Since immune cells other than mature macrophages might be recruited to a site of cell death, we also assessed expression of CD45 and found no evidence of T-cells, B-cells, dendritic cells, natural killer cells, monocytes, or granulocytes near jerboa foot myofibers from P4 to P8 (Figure 3E and Figure 3 – figure supplement 3).

The absence of any clear indication of muscle cell death motivated us to re-evaluate muscle maturation at greater resolution in order to capture the earliest detectable signs of muscle cell loss. We collected transmission electron micrographs of jerboa hand and foot muscle at P0, P2, and P4. We identified criteria for three categories of maturation, as described previously (Borisov et al., 2008; Raeker et al., 2014; Sanger et al., 2006), and two categories of degeneration. Category A cells have pre-myofibrils with thick and thin filaments and poorly resolved Z-discs, but the M-lines and I-bands are not yet apparent (Figure 4A). In Category B, Z-discs of nascent myofibrils are better resolved, and M-lines and I-bands are apparent, but parallel sarcomeres are not in register (Figure 4B). The mature myofibrils of Category C have Z-lines that are aligned with one another (Figure 4C). In Category D, early degeneration, some sarcomeres appear similar to Category A, but other areas of the cell contain disorganized filaments (Figure 4D). Category E includes those in the worst condition where less than half of the cell has any recognizable sarcomeres, and much of the cytoplasm is filled with pools of disorganized filaments and Z-protein aggregates (Figure 4E). Additionally, Category D and E cells have membrane-enclosed vacuoles and large lipid droplets (Figure 4 – figure supplement 1). However, consistent with a lack of evidence for cell death, none of these cells or their organelles appear swollen, nuclear morphology appears normal, plasma membranes seem to be contiguous, and we do not observe an accumulation of autophagic vesicles that typically characterize cell death associated with unregulated autophagy (Mizushima, 2007; Kroemer and Levine, 2008; Denton and Kumar, 2019).

We then coded and pooled all images of hand and foot myofibers from P0, P2, and P4 jerboas and blindly assigned each cell to one of the five categories. Quantification of the percent

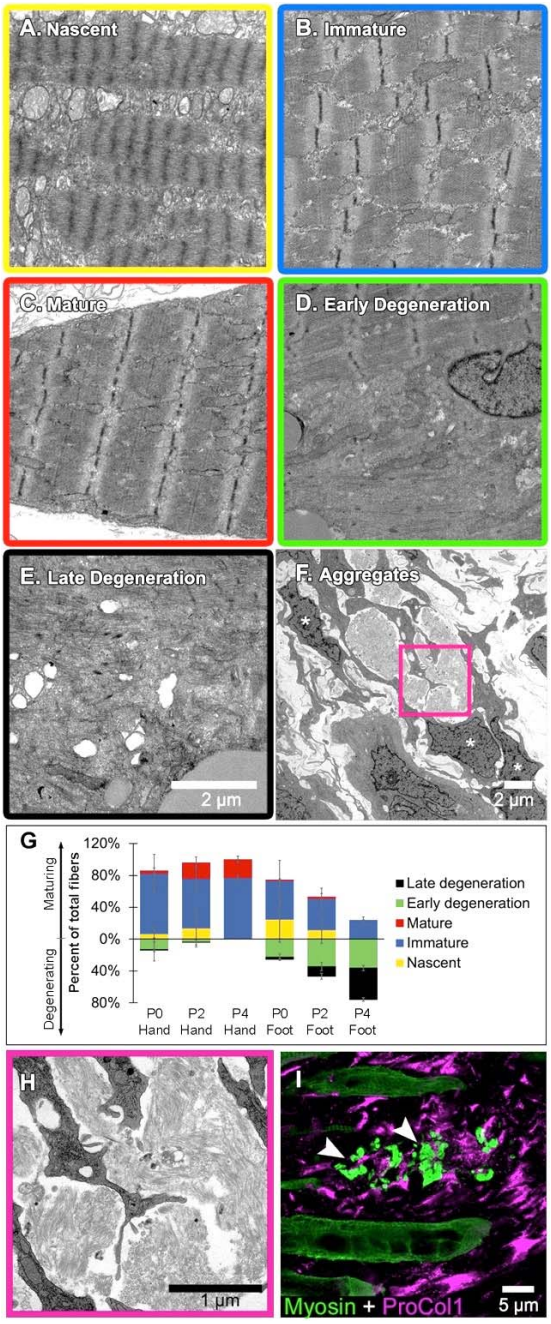

Figure 4: Jerboa foot myofibers degenerate from a nascent state soon after birth.

(A to C) TEM of representative jerboa hand myofibers illustrating categories (A) nascent, (B) immature, and (C) mature. (D and E) TEM of Representative jerboa foot myofibers illustrating categories (D) early degeneration and (E) late degeneration. Scale bar in E is also for A to D. (F) TEM of filamentous aggregates and surrounding fibroblast-like cells (asterisks) observed in jerboa feet. (G) Mean percentage and standard deviation of myofibers in each category in jerboa P0, P2, P4 hand and foot muscles. Number of myofibers pooled from three animals at each stage: hand – (P0), n=135; (P2), n=195; (P4), n=184 (P4); foot – (P0), n=186; (P2), n=193; (P4), n=186. (H) Higher magnification image of myofibril aggregates in F. (I) Pro-Collagen I positive cells surround skeletal muscle myosin^{+} aggregates (arrowheads) in jerboa feet. See also figure 4 – figure supplement 1.

of myofibers in each category after unblinding revealed the progressive maturation of jerboa hand myofibers and the progressive degeneration of jerboa foot myofibers (Figure 4G). Compared to later stages, there is little difference in the maturation state of hand and foot sarcomeres at birth. Loss of ultrastructural integrity is therefore initiated perinatally, prior to complete myofibril maturation in the jerboa foot.

Our analysis of transmission electron micrographs also revealed the presence of filamentous aggregates that we did not include in our quantifications because they are enucleate, lack all other recognizable organelles, and are not bounded by a plasma membrane. Although these aggregates do not appear to be cellular, they are always closely associated with cells of a fibroblast morphology, and most lie between remaining myofibers in a space we presume was also once occupied by a myofiber (Figure 4F,H). To determine if these unusual structures contain muscle protein, we performed immunofluorescence on sections of P4 jerboa foot muscle and found similar aggregates of intensely fluorescent immunoreactivity to skeletal muscle myosin heavy chain. We also found that the surrounding cells, which correlate with the positions of fibroblasts in electron micrographs, express the intracellular pro-peptide of Collagen I (Figure 4I), the major component of tendon and other fibrous connective tissues and of fibrotic tissue after injury (Mann et al., 2011).

Given the apparent deterioration of nascent sarcomeres, we asked whether individual sarcomere proteins are lost from myofibrils in a temporal order or if proteins disassemble simultaneously. We assessed the organization of sarcomere proteins by multicolor immunofluorescence at P0, P2, and P4. Alpha-Actinin, Desmin, Myomesin, Myosin, Titin, and Tropomyosin are each localized to an ordered series of striations in a subset of myofibers suggesting all are initially incorporated into immature sarcomeres (Figure 5A and Tables S1-5). By assessing all combinations of immunologically compatible primary antibodies, we identified populations of cells where Desmin was no longer present in an ordered array, but each of the other proteins appeared properly localized to the sarcomere (Figure 5B and Table S2). Although we could not distinguish such clear categories of mislocalization for each protein relative to all others, we inferred a relative timeline whereby Desmin disorganization is followed together by Myosin and Tropomyosin, then Titin, and lastly Myomesin and α-Actinin (Figure 5B-F and Tables S1-5).

Desmin forms a filamentous network that connects parallel sarcomeres to one another and coordinates myofibril contraction within cells and between neighboring cells (Bär et al., 2004; Capetanaki et al., 2015; Goldfarb et al., 2008). Mutations that cause desminopathies

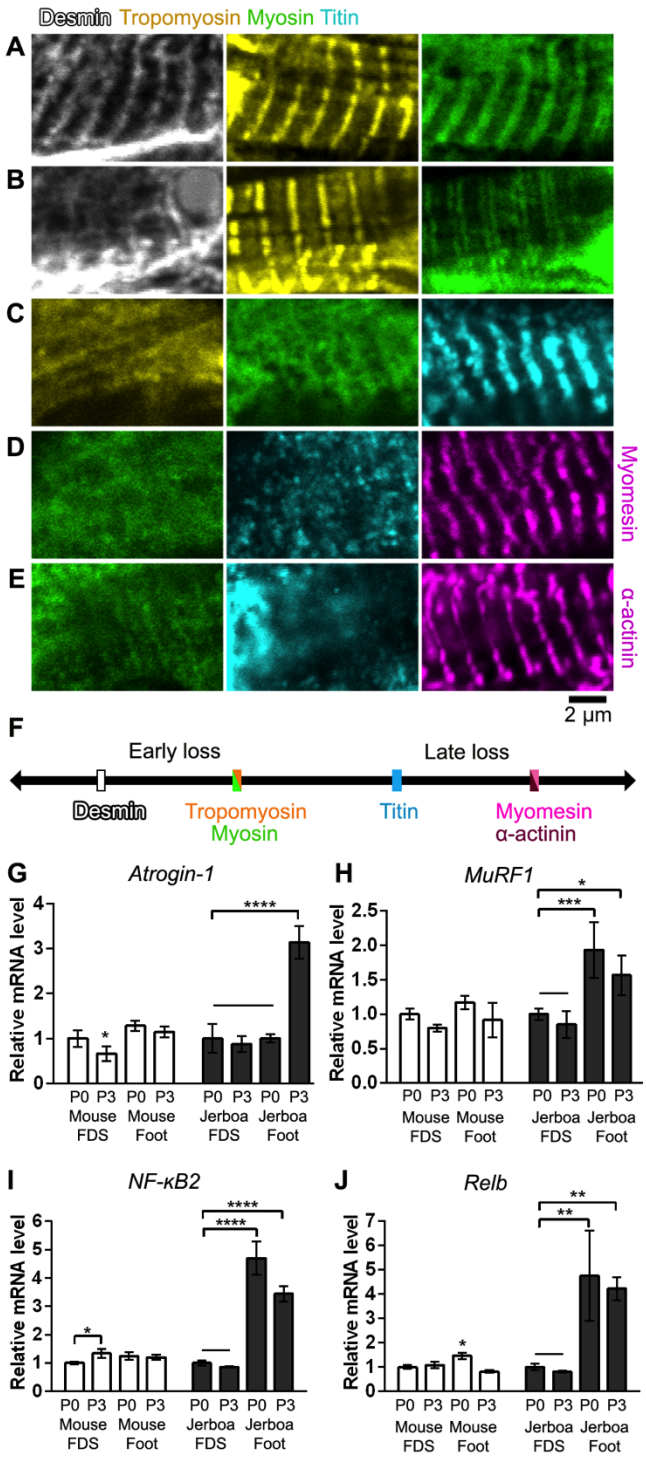

Figure 5: Sarcomere disorganization and E3 ubiquitin ligase expression suggest an 'atrophy-like' mechanism of jerboa foot muscle loss.

(A to E) Multicolor immunofluorescence images of sarcomere protein organization in P4 jerboa foot muscles (representative of 704 myofibers from seven P4 animals).
(F) Model of the interpreted order of sarcomere protein disorganization derived from Tables S1-5. (G and H) RT-qPCR measurements of (G) *Atrogin-1/MAFbx* and (H) *MuRF1* mRNA normalized to *SDHA*. Fold-change and standard deviations are expressed relative to the mean

for P0 forearm muscle (FDS) of the same species. Mouse P0 FDS (n=5), foot (n=4); mouse P3 FDS (n=3), foot (n4); jerboa P0 FDS (n=6), foot (n=5); jerboa P3 FDS (n=4), foot (n=6). In G: *p=0.0203, ****p<0.0001. In H: *p=0.0125, ***p=0.0002. (I and J) RT-qPCR measurements of (I) *NF-κB2* and (J) *Relb* mRNA normalized to *SDHA*. Fold-change and standard deviations are expressed relative to the mean for P0 forearm muscle (FDS) of the same species. Mouse P0 FDS (n=4), foot (n=3); mouse P3 FDS & foot (n=3); jerboa P0 FDS & foot (n=3); jerboa P3 FDS & foot (n=4). In I: *p=0.0112, ****p<0.0001. In J: *p=0.0473, **p=0.0017 & p=0.0032.

illustrate that Desmin is essential to maintain sarcomere integrity (Clemen et al., 2013). In mouse models of muscle atrophy triggered by fasting or denervation, phosphorylation of Desmin removes the protein from the sarcomere and targets it for ubiquitination and proteolytic degradation prior to degradation of other sarcomere proteins (Volodin et al., 2017). The observation that Desmin is the first of an ordered sarcomere disassembly in the jerboa foot may reflect targeted degradation of muscle proteins that is similar to muscle atrophy.

The ubiquitin-proteasome system is the main pathway through which cellular proteins are degraded during muscle atrophy, and *MuRF1* and *Atrogin-1* are E3 ubiquitin ligases among the 'atrogenes' that are highly upregulated (Bodine and Baehr, 2014; Schiaffino et al., 2013). To test the hypothesis that muscle loss in the jerboa foot exhibits molecular hallmarks of atrophy, we performed quantitative reverse transcriptase PCR (qRT-PCR) of *MuRF1* and *Atrogin-1* mRNA from intrinsic foot muscles and the *flexor digitorum superficialis* (FDS) of the mouse and jerboa. The FDS, which originates in the autopod during embryogenesis and translocates to the forearm (Huang et al., 2013), is the most easily dissected of the analogous forelimb muscles and serves as a control for typical muscle maturation in both species. When normalized to expression in the FDS at birth of each species, *Atrogin-1* expression is 3.1-fold higher in the jerboa foot at P3 (Figure 5G). *MuRF1* mRNA expression is already significantly elevated at birth and remains elevated at P3 (Figure 5H).

The NF-κB pathway is an upstream mediator of skeletal muscle atrophy (Li et al., 2008) and is both necessary and sufficient to induce *MuRF1* expression (Cai et al., 2004; Wu et al., 2014). To lend further support to the hypothesis that jerboa foot muscle loss involves an 'atrophy-like' mechanism, we performed qRT-PCR of *NF-κB2* and its binding partner, *Relb.* We observed that each gene is expressed greater than three-fold higher in jerboa foot at birth and at P3 (Figure 5 – figure supplement 1A, B). The progressively disordered ultrastructure of the sarcomere that begins with loss of Desmin localization, the increased expression of multiple genes that are typically upregulated during atrophy, and the lack of evidence for cell death or macrophage infiltration are consistent with observations of atrophying muscle in mice and rats

(Volodin et al., 2017; Bonaldo and Sandri, 2013; Sakuma et al., 2015; von Haehling et al., 2010).

Despite the similarities to muscle atrophy, myofiber loss in the jerboa foot does not seem to be simply explained by an atrophic response to denervation. First, and in contrast to the rapid rate of jerboa foot myofiber loss, chronic denervation in mice (100 days after nerve transection at P14) reduced the size but not the number of individual myofibers (Moschella and Ontell, 1987a). Additionally, we found that the post-synaptic Acetylcholine Receptor (AchR) exclusively coincides with the presynaptic neuronal protein, Synaptophysin, in neonatal jerboa foot muscles (Figure 5 – figure supplement 1). In the mouse, AchR clusters are present in a broad domain of fetal muscle prior to innervation and are refined to nerve terminals in response to chemical synapse activity before birth (Yang et al., 2001). The refinement of AchR clusters in jerboa foot muscles suggests that the muscles are not only innervated at birth but are also responsive to motor inputs.

Discussion

The natural process of muscle loss in the jerboa foot is surprising in the context of what is known about muscle development and pathology. Although we found multinucleated myofibers in the feet of neonatal jerboas, all muscle protein expression rapidly disappears from the jerboa foot shortly after birth. We were perplexed to find no evidence of apoptotic or necrotic cell death by a variety of assays and throughout the time when muscle cells are lost, nor did we observe immune cells that are commonly recruited to clear the remains of dying cells. Instead, we saw structural and molecular similarities to muscle atrophy, though atrophy in young mice leads to reduced myofiber size rather than number as in the jerboa (Bruusgaard and Gundersen, 2008; Moschella and Ontell, 1987a).

As for why the phenotype is limited to the distal limb, it is possible that disuse contributes to jerboa foot muscle loss, since jerboas and ungulates each fuse metatarsals into a single cannon bone, which would be expected to physically impair lateral motion of the digit elements (Cunningham, 1883; Moore et al., 2015). However, the rapid and complete loss of myofibers in the neonatal jerboa foot does not appear to simply reflect a species-level difference in the animal's generalized response to disuse atrophy, since hindlimb denervation and immobilization in adults causes gradual loss of muscle mass, primarily through a significant reduction in the diameter of individual myofibers (AlWohaib and Alnaqeeb, 1997; Aryan and Alnaqeeb, 2002). These observations are very similar to what has been shown in disuse atrophy models in mice

and in rats (Bonaldo and Sandri, 2013; Moschella and Ontell, 1987b) and differ from what we see in the neonatal foot.

Why would an embryo expend energy to form muscles that are almost immediately lost? The formation and subsequent loss of intrinsic foot muscles in jerboas and hooved animals may simply reflect a series of chance events in each lineage with no fitness cost, or these similarities in multiple species may reveal true developmental constraints. Muscle is not required for autopod tendon formation or maintenance in mice, but the tendons that develop in a muscle-less or a paralyzed mouse are thinner and less well organized (Huang et al., 2015). It is therefore possible that muscle is initially required in the fetus and neonate for tendons to establish sufficient architecture from origin to insertion so that the tendon, after further growth, can withstand high locomotor forces in the adult (Lochner et al., 1980; Moore et al., 2017).

Regardless of whether these nascent muscles serve an essential purpose, we are left wondering what is the ultimate fate of jerboa foot myofibers. If these cells do indeed die, perhaps death is too rapid for detection. However, programmed cell death is thought to occur over hours or even days from the initial trigger to the final corpse (Green, 2005). Alternatively, death may result from a mechanism that does not proceed through DNA fragmentation, plasma membrane permeability, macrophage recruitment, or stereotyped ultrastructural changes, and yet this would seem to eliminate most known forms of regulated cell death (Galluzzi et al., 2007)

Alternatively, multinucleated myofibers may transform to another cellular identity after degrading all sarcomere proteins. Although a fate transformation would be surprising, it would not be without precedent. The electric organ of fish that can produce an electric field (e.g. knifefish and elephantfish) is thought to be derived from skeletal muscle. Electrocytes of *Sternopygus macrurus* express skeletal muscle Actin, Desmin, and α-Actinin, and electrocytes of *Paramormyrops kingsleyae* retain sarcomeres that are disarrayed and non-contractile (Gallant et al., 2014; Unguez and Zakon, 1998). If myofibers in the jerboa foot indeed transdifferentiate, it is possible they transform into the pro-Collagen I positive fibroblasts that are entangled with the filamentous aggregates, though these could also be phagocytic fibroblasts recruited to consume the enucleate detritus without stimulating inflammation (Heredia et al., 2013; Joe et al., 2010; Monks et al., 2005; Schwegler et al., 2015). Unfortunately, the lineage labeling approaches required to track the ultimate fate of jerboa myofibers are exceptionally challenging in this non-traditional animal model.

It is clear, however, that regardless of the ultimate fate of jerboa foot myofibers, their path passes through a phase marked by cell biology that is typical of atrophy, including the ordered disassembly of sarcomeres and expression of the E3 ubiquitin ligases, *MuRF1* and

Atrogin-1. However, skeletal muscle atrophy is typically associated with pathology in the context of disuse, nerve injury, starvation, or disease. In this context, we were struck by a statement in the 1883 anatomical description of the fetal and adult suspensory ligament of four species of hooved mammals: “It is an instance of *pathological* change assisting a *morphological* process” (emphasis his) (Cunningham, 1883). Indeed, there are remarkable similarities in the histology of jerboa and horse foot muscle compared to human clinical observations of tissue remodeling that follows rotator cuff tear characterized by muscle atrophy, myofiber loss, and fibrosis (Souza et al., 2010; Gibbons et al., 2017).

Foot muscle atrophy in the jerboa may be one of many cellular responses associated with injury or disease in humans that is utilized in the normal development and physiology of other species. These data suggest that there is less of a clear divide between natural and pathological states than typically thought. Studies of non-traditional species may not only reveal the mechanisms of evolutionary malleability, but may also advance our understanding of fundamental biological processes that are typically associated with pathological conditions.

Materials and Methods

Animals

Jerboas were housed and reared as previously described (Jordan et al., 2011). CD1 mice were obtained from Charles River Laboratories (MA, USA), housed in standard conditions, and fed a breeder’s diet. All animal care and use protocols for mice and jerboas were approved by the Institutional Animal Care and Use Committee (IACUC) of the University of California, San Diego.

Antibodies

The following primary antibodies and dilutions were used for immunofluorescence of tissue sections: Col1A1 (SP1.D8, 1:20), Dystroglycan (11H6C4, 1:10), Myosin heavy chain (MF20, 1:20), Myomesin (B4, 1:20), Myogenin (F5D, 1:5), Titin (9D10, 1:10), Tropomyosin (CH1, 1:10), Developmental Studies Hybridoma Bank; Desmin (D33, 1:300), α-actinin (EA-53, 1:1000), Sigma Aldrich; Annexin-V (ab14196, 1:100), Desmin (ab8592, 1:500), CD45 (ab10558, 1:200), F4/80 (ab6640, 1:200), Abcam; Cleaved Caspase-3 (Asp175) (#9661, 1:100), Cell Signaling Technologies; Alexa 488 conjugated Wheat Germ Agglutinin (W11261, 1:200), Invitrogen; BrdU (MCA2060, 1:100), Biorad.

Secondary antibodies were obtained from Invitrogen and used at 1:250 dilution: Alexa Fluor 594 conjugated goat anti-mouse IgG2b, Alexa Fluor 488 or 647 conjugated goat anti-

mouse IgG1, Alexa Fluor 488 conjugated goat anti-mouse IgM, Alexa Fluor donkey anti-mouse IgG, Alexa Fluor 488 conjugated goat anti-rat IgG, Alexa Fluor 488 or 647 conjugated goat anti-rabbit.

Immunofluorescence and TUNEL

Mouse and jerboa limbs were dissected and fixed in 4% PFA in 1x PBS overnight. Tissues were washed in 1X PBS twice for 20 min and placed in 30% sucrose in 1x PBS overnight at 4 degrees Celsius. Tissues were then mounted in a cryomold in OCT freezing media, and blocks were frozen and stored at -80°C until cryosectioned.

Blocks were sectioned at 12 µm thickness, and sections were transferred to Super-Frost Plus slides (Thermo Fisher). For immunofluorescence, slides were washed for 5 min in 1x PBS and subject to antigen retrieval by incubation in Proteinase K (5 µg/mL) for 10 min followed by 5 min postfix in 4% PFA in PBS and three washes in 1x PBS. Slides were then blocked in a solution of 5% heat inactivated goat serum, 3% Bovine Serum Albumin, 0.1% TritonX-100, 0.02% SDS in PBS. Slides were incubated in the appropriate primary antibody dilution in block overnight at 4°C. On the second day, slides were washed three times for 10 minutes in PBST (1x PBS + 0.1% TritonX-100) and incubated at room temperature in secondary antibodies and 1 µg/ml DAPI for one hour. Slides were then washed three times for 10 minutes in PBST and mounted in Fluoro Gel with DABCO (EMS).

For TUNEL, slides that had been previously processed for MF20 immunofluorescence were placed immediately into the TUNEL reaction mixture following manufacturer's instructions (Roche In Situ Cell Death Detection Kit, TM-Red) for 60 min at 37°C, rinsed three times in 1x PBS, and mounted in Fluoro Gel with DABCO.

Sections were imaged with Olympus compound microscope model BX61, Leica SP5 confocal, or Olympus FV1000 confocal.

Myofiber count

Blocks containing embedded mouse or jerboa feet were cryosectioned at 12µm thickness in transverse orientation onto two serial sets of slides. Slides of the second series were used as back up in case certain sections of the first series contain folded tissue and thus cannot be used. Slides of the first series were stained with MF20 & WGA and analyzed to locate the proximal and distal ends of the third interosseous muscle. Using this information we estimated the middle area of each muscle and selected 10 sections for subsequent analysis. We analyzed the third interosseous muscle of the hindlimb, spanning approximately

240 µm in muscle length. For each selected section, all cross-sectionally oriented myofibers were manually counted and recorded using the plugin cell counter in ImageJ. The average number of myofibers from 10 sections represents an estimate of the myofiber number for the middle transverse section of the third interosseous muscle. For each developmental stage, data from three animals were collected, and one-way ANOVA with Tukey's multiple comparisons test was performed to determine the statistical significance of mean myofiber number differences between developmental stages in each species.

Myocyte fusion assay

BrdU solution was intraperitoneally injected to achieve 100 µg/g (BrdU/ animal body weight) in P0, P2, and P4 jerboas. Injected animals were sacrificed two days later. The feet and hands of each animal were fixed in 4% PFA/PBS overnight, processed through a sucrose series, and embedded in OCT freezing media. Blocks of embedded tissue were cryosectioned in transverse orientation at 12 µm thickness and placed in serial sets on Superfrost Plus slides. Slides were stained with BrdU and Dystroglycan antibodies as indicated above. As in the methods to count myofibers, we chose ten sections near the midpoint of the interosseous muscle associated with the third metatarsal and counted all BrdU+ nuclei within a Dystroglycan+ myofiber as well as all myofiber nuclei in each section. Data is represented as the total number of BrdU+ myofiber nuclei divided by the total number of myofiber nuclei, and this ratio was averaged for all 10 sections in each animal. The data was plotted using Prism8 (GraphPad), and the statistical significance between datapoints at each time interval was calculated with one-way ANOVA with Tukey's multiple comparisons test in each of forelimb and hindlimb.

Short-term BrdU labeling

BrdU solution was intraperitoneally injected to achieve 100 µg/g (BrdU/ animal body weight) in P0, P2, and P4 jerboas. Injected animals were sacrificed two hours after injection. The feet and hands of each animal were fixed in 4% PFA/PBS overnight, processed through a sucrose series, and embedded in OCT freezing media. Blocks of embedded tissue were cryosectioned in transverse orientation at 12 µm thickness and placed in serial sets on Superfrost Plus slides. Slides were stained with BrdU and Myosin or BrdU, Laminin, and Dystroglycan antibodies as indicated above for assessment of proliferation in myonuclei. As in the methods of fusion assay, we chose ten sections near the midpoint of the interosseous muscle associated with the third metatarsal and counted all BrdU+ nuclei within a Laminin+ basal lamina and outside Dystroglycan+ myofiber membrane as well as number of

Dystroglycan+ myofiber in each section. Data is represented as the total number of BrdU+ myofiber nuclei divided by the total number of myofiber, and this ratio was averaged for all 10 sections in each animal. The data was plotted using Prism8 (GraphPad), and the statistical significance between datapoints at each time interval was calculated with one-way ANOVA with Tukey's multiple comparisons test in each of forelimb and hindlimb.

Muscle stem/progenitor cell culture:

Intrinsic foot muscles (*m. flexor digitorum brevis* and *m. interossei*) and lower leg muscles (*tibialis anterior* and *gastrocnemius*) were manually dissected from three animals of P1 jerboas and mice and pooled. After connective tissues were manually removed with forceps, muscle stem/progenitor cells were isolated and cultured as described in (Danoviz and Yablonka-Reuveni, 2012b) Briefly, the tissues were enzymatically with 10 mg/ml Pronase (EMD Millipore) and mechanically dissociated. The cells were plated onto matrigel-coated 8-well chamber slides (Nunc Lab-Tek, Thermo fisher) coated with Matrigel (Corning) at 1×10^4 cells/well. The cells were cultured for 9 days with DMEM (Thermo Fisher), 20% fetal bovine serum (Thermo fisher), 10% horse serum (Thermo Fisher) and 1% chicken embryonic extract (Accurate Chemical). During the culture period, the medium was changed at day 3, 6, and 8. After 6 and 9 days, cells in replicate cultured wells were fixed with 4% PFA/PBS at 4℃ for 15 min and washed with PBS. After permeabilization with 1 % Triton-X 100 in PBS at room temperature for 10 min, the cells were blocked with 5% BSA/PBS for 30 min and stained with BrdU, anti-Myogenin and Myosin antibodies and secondary antibodies. At each time point of each experimental group, the total number of nuclei and nuclei within Myosin+ myofibers were counted in 10 images taken from 8 wells using the Olympus compound microscope at 4x magnification. The numbers in 10 images were averaged and the difference between day 6 and day 9 were statistically analyzed with paired sample t-test in each experimental group.

Evans Blue Dye

We injected Evans Blue Dye as 1% solution by animal body weight (1mg EBD/100µl PBS/10g) 24 hours prior to sample collection (Hamer et al., 2002). As a positive control for EBD uptake, we create an injured muscle area by inserting a 21-gauge needle 2-3 times into the jerboa gastrocnemius muscle. Samples were fresh frozen in OCT and cryosection at 12 µm thickness. Slides were processed for MF20 fluorescence with primary antibody incubation for 1 hr at RT before secondary antibody incubation. Slides were mounted for analysis: EBD signal is

detected using the Cy5 filter and imaged using the Olympus compound microscope or imaged using the Leica SP5 confocal laser 633nm.

Oil red O (ORO) staining

ORO stock solution: 2.5 g of Oil red O to 400 ml of 99% (vol/vol) isopropyl alcohol and mix the solution by magnetic stirring for 2 h at room temperature (RT; 20–25 °C). ORO working solution: 1.5 parts of ORO stock solution to one part of deionized (DI). Cryosections were fixed with 4%PFA in 1x PBS for 5 minutes. Slides were washed with 2x with PBS for 10 minutes each and stained with ORO working solution for 10 minutes followed three 30 second washes with DI water. Slides were then washed in running tap water for 15 minutes followed by three 30 second washes with DI water and mounting in aqueous medium.

Transmission Electron Microscopy (TEM)

Animals were perfused with 2% glutaraldehyde and 2% PFA plus 2mM $CaCl_2$ in 0.15M sodium cacodylate buffer, pH 7.4 @ 35°C for 2-3 minutes. The hands and feet were removed, skinned, and fixed on ice for 2 hours. Samples were then rinsed six times for 5 min in cold 0.15M cacodylate buffer and then post-fixed in 1% OsO4 in 0.15M cacodylate buffer on ice for 1 hour. Samples were then rinsed in cold double distilled water (DDW) six times for 5 min and placed into 1% uranyl acetate in DDW on ice overnight. Fixed tissue was then rinsed in ice cold double distilled water three times for 3 min and dehydrated in an ethanol series (50%, 70%, 90% in DDW) on ice for 5 min each. Samples were further dehydrated into 100% ethanol twice for 5 min at room temperature and then transitioned to 1:1 ethanol:acetone for 5 min followed by two times 5 min in 100% acetone. Dehydrated samples were infiltrated with 1:1 acetone:Durcupan ACM resin for 1 hour at room temperature followed by 100% resin twice for 1 hour and then placed in fresh resin overnight. On the next day, samples were transferred to fresh resin, which was polymerized in a 60°C vacuum oven for 48-72 hours. Resin embedded samples were stored at room temperature until ready for sectioning. Seventy nanometer thick sections were stained in lead solution and image using Tecnai Spirit TEM scope (120 kV).

RNA isolation and quantitative reverse transcriptase polymerase chain reaction (qRT-PCR)

Foot muscles were dissected and stored in RNAlater solution (Thermo Fisher) at -80°C until ready for use. RNA extraction was performed using the PicoPure RNA Isolation Kit (Thermo Fisher) according to the manufacture instructions. RNA was reverse transcribed to

generate cDNA using QuantiTect Reverse Transcription Kit. cDNA was used as template for quantitative PCR with PCR amplification detected with Sybr green (SYBR Green Real-time PCR master mixes, Invitrogen). See the table below for the sequences of primers used to quantify real time amplification.

Each quantitative reverse transcriptase PCR experiment was conducted twice with technical triplicates in each experiment. Cq values that are significant outliers were determined using Grubb's test in GraphPad software and eliminated. Expression of *MuRF-1*, *Atrogin-1, NF-κB2, and Relb* was normalized to *SDHA,* quantitation of gene expression was determined by the equation $2^{-\Delta\Delta CT}$, and the fold-change of mRNA expression was calculated relative to the mRNA level of P0 FDS samples in each species, which was set to 1. One-way ANOVA with Tukey's multiple comparisons test was performed to determine the statistical significance of fold change differences between samples in each species.

mouseMuRF1_F	TGCCTGGAGATGTTTACCAAGC	(Dogra et al., 2007)
mouseMuRF1_R	AAACGACCTCCAGACATGGACA	(Dogra et al., 2007)
mouseAtrogin_F	TGGGTGTATCGGATGGAGAC	(Files et al., 2012)
mouseAtrogin_R	TCAGCCTCTGCATGATGTTC	(Files et al., 2012)
jerboaMuRF1_F	CCGCGTGCAGACTATCATCA	
jerboaMuRF1_R	GCAGCTCGCTCTTTTTCTCG	
jerboaAtrogin_F	GCATCGCCCAAAAGAACTTCA	
jerboaAtrogin_R	ACTTGCCGACTCTTTGGACC	
mouseSDHA_F	GGAACACTCCAAAAACAGACCT	(Xu et al., 2016)
mouseSDHA_R	CCACCACTGGGTATTGAGTAGAA	(Xu et al., 2016)
jerboaSDHA_F	ACTGGAGGTGGCATTTCTAC	
jerboaSDHA_R	TTTTCTAGCTCGACCACAGATG	
mouseNF-κB2_F	GCCCAGCACAGAGGTGAAAG	
mouseNF-κB2_R	CATTCAGTGCACCTGAGGCT	
mouseRelb_F	TGTCACTAACGGTCTCCAGGAC	
mouseRelb_R	CAGGCGCGGCATCTCACT	
jerboaNF-κB2_F	CTAGCCCACAGACATGGACA	
jerboaNF-κB2_R	TAGGGGCCATCAGCTGTCTC	
jerboaRelb_F	CCTACAATGCTGGCTCTCTGA	
jerboaRelb_R	GTCATAGACAGGCTCGGACA	

Acknowledgements

We thank V. Fowler, S. Lange, A. Sacco, S. Ward, D. Gokhin and R. Nowak for advice and for sharing reagents. M. Ellisman, Director of the National Center for Microscopy and Imaging Research at UC San Diego (P41 GM103412), T. Deerinck, M. Mackey, and A. Thor provided assistance with transmission electron microscopy. Access to the Olympus FV1000 was provided by the UC San Diego School of Medicine Microscopy Core (NINDS NS047101). H.

Grunwald assisted with TUNEL staining. A. Mendelsohn provided advice on the assessment of muscle innervation, and Y. Cho advised us on mouse muscle denervation. Multiple monoclonal antibodies used in this project were obtained from the Developmental Studies Hybridoma Bank, created by the NICHD of the NIH and maintained at The University of Iowa, Department of Biology. This work was funded by a Searle Scholar Award from the Kinship Foundation, a Pew Biomedical Scholar Award from the Pew Charitable Trusts, a Packard Fellowship in Science and Engineering from the David and Lucile Packard Foundation and NIH grant R21AR074609 from the National Institutes of Arthritis and Musculoskeletal and Skin Diseases (NIAMS). M.P.T. was supported by the NIH Cell and Molecular Genetics training grant T32GM724039.

References

Abdala, V., Grizante, M.B., Diogo, R., Molnar, J., and Kohlsdorf, T. (2015). Musculoskeletal anatomical changes that accompany limb reduction in lizards. Journal of Morphology *276*, 1290–1310.

Abmayr, S.M., and Pavlath, G.K. (2012). Myoblast fusion: lessons from flies and mice. Development *139*, 641–656.

AlWohaib, M.A., and Alnaqeeb, M.A. (1997). The effect of denervation and immobilization on the hindlimb muscles of the jerboa (Jaculus jaculus). Kuwait J. Sci. Eng. *24*, 309–323.

Arnold, L., Henry, A., Poron, F., Baba-Amer, Y., van Rooijen, N., Plonquet, A., Gherardi, R.K., and Chazaud, B. (2007). Inflammatory monocytes recruited after skeletal muscle injury switch into antiinflammatory macrophages to support myogenesis. The Journal of Experimental Medicine *204*, 1057–1069.

Aryan, F.A., and Alnaqeeb, M.A. (2002). Effect of immobilization and under-load on skeletal muscle in the Hindlimb of the Jerboa. Kuwait J. Sci. Eng. *29*, 83–97.

Bär, H., Strelkov, S. V, Sjöberg, G., Aebi, U., and Herrmann, H. (2004). The biology of desmin filaments: how do mutations affect their structure, assembly, and organisation? Journal of Structural Biology *148*, 137–152.

Berghe, T. Vanden, Linkermann, A., Jouan-Lanhouet, S., Walczak, H., and Vandenabeele, P. (2014). Regulated necrosis: the expanding network of non-apoptotic cell death pathways. Nature Reviews Molecular Cell Biology *15*, 135–147.

Berman, S.L. (1985). Convergent evolution in the hindlimb of bipedal rodents. Journal of Zoological Systematics and Evolutionary Research *23*, 59–77.

Bodine, S.C., and Baehr, L.M. (2014). Skeletal muscle atrophy and the E3 ubiquitin ligases MuRF1 and MAFbx/atrogin-1. American Journal of Physiology. Endocrinology and Metabolism *307*, E469-84.

Bodine, S.C., Latres, E., Baumhueter, S., Lai, V.K., Nunez, L., Clarke, B.A., Poueymirou, W.T., Panaro, F.J., Na, E., Dharmarajan, K., et al. (2001). Identification of ubiquitin ligases required for skeletal muscle atrophy. Science (New York, N.Y.) *294*, 1704–1708.

Bonaldo, P., and Sandri, M. (2013). Cellular and molecular mechanisms of muscle atrophy. Disease Models & Mechanisms *6*, 25–39.

Bönnemann, C.G., and Laing, N.G. (2004). Myopathies resulting from mutations in sarcomeric proteins. Current Opinion in Neurology *17*, 529–537.

Borisov, A.B., Martynova, M.G., and Russell, M.W. (2008). Early incorporation of obscurin into nascent sarcomeres: implication for myofibril assembly during cardiac myogenesis. Histochemistry and Cell Biology *129*, 463–478.

Botelho, J.F., Smith-Paredes, D., Nuñez-Leon, D., Soto-Acuña, S., and Vargas, A.O. (2014). The developmental origin of zygodactyl feet and its possible loss in the evolution of Passeriformes. Proc Biol Sci *281*.

Brill, A., Torchinsky, A., Carp, H., and Toder, V. (1999). The Role of Apoptosis in Normal and Abnormal Embryonic Development. J Assist Reprod Genet *16*, 512–519.

Bruusgaard, J.C., and Gundersen, K. (2008). In vivo time-lapse microscopy reveals no loss of murine myonuclei during weeks of muscle atrophy. J. Clin. Invest. *118*, 1450–1457.

Cai, D., Frantz, J.D., Tawa, N.E., Melendez, P.A., Oh, B.-C., Lidov, H.G.W., Hasselgren, P.-O., Frontera, W.R., Lee, J., Glass, D.J., et al. (2004). IKKbeta/NF-kappaB activation causes severe muscle wasting in mice. Cell *119*, 285–298.

Capetanaki, Y., Papathanasiou, S., Diokmetzidou, A., Vatsellas, G., and Tsikitis, M. (2015). Desmin related disease: A matter of cell survival failure. Current Opinion in Cell Biology *32*, 113–120.

Chevallier, A., Kieny, M., and Mauger, A. (1977). Limb-somite relationship: origin of the limb musculature. Journal of Embryology and Experimental Morphology *41*, 245–258.

Chiakulas, J.J., and Pauly, J.E. (1965). A study of postnatal growth of skeletal muscle in the rat. The Anatomical Record *152*, 55–61.

Christ, B., Jacob, H.J., and Jacob, M. (1977). Experimental analysis of the origin of the wing musculature in avian embryos. Anatomy and Embryology *150*, 171–186.

Clemen, C.S., Herrmann, H., Strelkov, S.V., and Schröder, R. (2013). Desminopathies: pathology and mechanisms. Acta Neuropathol. *125*, 47–75.

Cunningham, D.J. (1883). The Development of the Suspensory Ligament of the Fetlock in the Foetal Horse, Ox, Roe-Deer, and Sambre-Deer. Journal of Anatomy and Physiology *18*, i1-12.

Danoviz, M.E., and Yablonka-Reuveni, Z. (2012a). Skeletal Muscle Satellite Cells: Background and Methods for Isolation and Analysis in a Primary Culture System. In Myogenesis: Methods and Protocols, J.X. DiMario, ed. (Totowa, NJ: Humana Press), pp. 21–52.

Danoviz, M.E., and Yablonka-Reuveni, Z. (2012b). Skeletal muscle satellite cells: background and methods for isolation and analysis in a primary culture system. Methods Mol. Biol. *798*, 21–52.

Denton, D., and Kumar, S. (2019). Autophagy-dependent cell death. Cell Death & Differentiation *26*, 605.

Dogra, C., Changotra, H., Wedhas, N., Qin, X., Wergedal, J.E., and Kumar, A. (2007). TNF-related weak inducer of apoptosis (TWEAK) is a potent skeletal muscle-wasting cytokine. FASEB Journal : Official Publication of the Federation of American Societies for Experimental Biology *21*, 1857–1869.

Ehler, E., and Gautel, M. (2008). The Sarcomere and Sarcomerogenesis. In The Sarcomere and Skeletal Muscle Disease, N.G. Laing, ed. (New York, NY: Springer New York), pp. 1–14.

Elmore, S. (2007). Apoptosis: a review of programmed cell death. Toxicologic Pathology *35*, 495–516.

Fernández-Terán, M. a, Hinchliffe, J.R., and Ros, M. a (2006). Birth and death of cells in limb development: a mapping study. Developmental Dynamics : An Official Publication of the American Association of Anatomists *235*, 2521–2537.

Files, D.C., D'Alessio, F.R., Johnston, L.F., Kesari, P., Aggarwal, N.R., Garibaldi, B.T., Mock, J.R., Simmers, J.L., DeGorordo, A., Murdoch, J., et al. (2012). A Critical Role for Muscle Ring Finger-1 in Acute Lung Injury–associated Skeletal Muscle Wasting. American Journal of Respiratory and Critical Care Medicine *185*, 825–834.

Furst, D.O., Fürst, D.O., Osborn, M., and Weber, K. (1989). Myogenesis in the mouse embryo: differential onset of expression of myogenic proteins and the involvement of titin in myofibril assembly. The Journal of Cell Biology *109*, 517–527.

Gallant, J.R., Traeger, L.L., Volkening, J.D., Moffett, H., Chen, P.-H., Novina, C.D., Phillips, G.N., Anand, R., Wells, G.B., Pinch, M., et al. (2014). Nonhuman genetics. Genomic basis for the convergent evolution of electric organs. Science (New York, N.Y.) *344*, 1522–1525.

Galluzzi, L., Maiuri, M.C., Vitale, I., Zischka, H., Castedo, M., Zitvogel, L., and Kroemer, G. (2007). Cell death modalities: classification and pathophysiological implications. Cell Death and Differentiation *14*, 1237–1243.

Gibbons, M.C., Singh, A., Anakwenze, O., Cheng, T., Pomerantz, M., Schenk, S., Engler, A.J., and Ward, S.R. (2017). Histological Evidence of Muscle Degeneration in Advanced Human Rotator Cuff Disease. J Bone Joint Surg Am *99*, 190–199.

Gokhin, D.S., Ward, S.R., Bremner, S.N., and Lieber, R.L. (2008). Quantitative analysis of neonatal skeletal muscle functional improvement in the mouse. J. Exp. Biol. *211*, 837–843.

Goldfarb, L.G., Olive, M., Vicart, P., and Goebel, H.H. (2008). Intermediate filament diseases: desminopathy. In The Sarcomere and Skeletal Muscle Disease, N.G. Laing, ed. (New York, NY: Landes Biosciences and Springer Science+Business Media, LLC), pp. 131–160.

Green, D.R. (2005). Apoptotic Pathways: Ten Minutes to Dead. Cell *121*, 671–674.

von Haehling, S., Morley, J.E., and Anker, S.D. (2010). An overview of sarcopenia: facts and numbers on prevalence and clinical impact. J Cachexia Sarcopenia Muscle *1*, 129–133.

Hamer, P.W., McGeachie, J.M., Davies, M.J., and Grounds, M.D. (2002). Evans Blue Dye as an in vivo marker of myofibre damage: optimising parameters for detecting initial myofibre membrane permeability. Journal of Anatomy *200*, 69–79.

Hayashi, K., and Ozawa, E. (1991). Vital labelling of somite-derived myogenic cells in the chicken limb bud. Roux's Archives of Developmental Biology *200*, 188–192.

Heredia, J.E., Mukundan, L., Chen, F.M., Mueller, A.A., Deo, R.C., Locksley, R.M., Rando, T.A., and Chawla, A. (2013). Type 2 innate signals stimulate fibro/adipogenic progenitors to facilitate muscle regeneration. Cell *153*, 376–388.

Huang, A.H., Riordan, T.J., Wang, L., Eyal, S., Zelzer, E., Brigande, J.V., and Schweitzer, R. (2013). Re-positioning forelimb superficialis muscles: tendon attachment and muscle activity enable active relocation of functional myofibers. Dev Cell *26*, 544–551.

Huang, A.H., Riordan, T.J., Pryce, B., Weibel, J.L., Watson, S.S., Long, F., Lefebvre, V., Harfe, B.D., Stadler, H.S., Akiyama, H., et al. (2015). Musculoskeletal integration at the wrist underlies the modular development of limb tendons. Development *142*, 2431–2441.

Hudson, G.E. (1937). Studies on the Muscles of the Pelvic Appendage in Birds. The American Midland Naturalist *18*, 1–108.

Joe, A.W.B., Yi, L., Natarajan, A., Le Grand, F., So, L., Wang, J., Rudnicki, M.A., and Rossi, F.M. V. (2010). Muscle injury activates resident fibro/adipogenic progenitors that facilitate myogenesis. Nature Cell Biology *12*, 153–163.

Jordan, B., Vercammen, P., and Cooper, K.L. (2011). Husbandry and breeding of the lesser Egyptian Jerboa, Jaculus jaculus. Cold Spring Harbor Protocols *2011*, 1457–1461.

Kardon, G. (1998). Muscle and tendon morphogenesis in the avian hind limb. Development *125*, 4019–4032.

Kardon, G., Harfe, B.D., and Tabin, C.J. (2003). A Tcf4-positive mesodermal population provides a prepattern for vertebrate limb muscle patterning. Dev. Cell *5*, 937–944.

Kelly, A.M., and Zacks, S.I. (1969). The histogenesis of rat intercostal muscle. The Journal of Cell Biology *42*, 135–153.

Kroemer, G., and Levine, B. (2008). Autophagic cell death: the story of a misnomer. Nat Rev Mol Cell Biol *9*, 1004–1010.

Krull, C.E. (2004). A primer on using in ovo electroporation to analyze gene function. Developmental Dynamics *229*, 433–439.

Labeit, S., Kohl, C.H., Witt, C.C., Labeit, D., Jung, J., and Granzier, H. (2010). Modulation of muscle atrophy, fatigue and MLC phosphorylation by MuRF1 as indicated by hindlimb suspension studies on MuRF1-KO mice. J. Biomed. Biotechnol. *2010*, 693741.

Laing, N.G., and Nowak, K.J. (2005). When contractile proteins go bad: the sarcomere and skeletal muscle disease. BioEssays : News and Reviews in Molecular, Cellular and Developmental Biology *27*, 809–822.

Li, H., Malhotra, S., and Kumar, A. (2008). Nuclear Factor-kappa B Signaling in Skeletal Muscle Atrophy. J Mol Med (Berl) *86*, 1113–1126.

Lochner, F.K., Milne, D.W., Mills, E.J., and Groom, J.J. (1980). In vivo and in vitro measurement of tendon strain in the horse. Am. J. Vet. Res. *41*, 1929–1937.

Londhe, P., and Guttridge, D.C. (2015). Inflammation induced loss of skeletal muscle. Bone *80*, 131–142.

Magerl, M., Tobin, D.J., Müller-Röver, S., Hagen, E., Lindner, G., McKay, I.A., and Paus, R. (2001). Patterns of Proliferation and Apoptosis during Murine Hair Follicle Morphogenesis. Journal of Investigative Dermatology *116*, 947–955.

Mann, C.J., Perdiguero, E., Kharraz, Y., Aguilar, S., Pessina, P., Serrano, A.L., and Muñoz-Cánoves, P. (2011). Aberrant repair and fibrosis development in skeletal muscle. Skelet Muscle *1*, 21.

Matsuda, R., Nishikawa, A., and Tanaka, H. (1995). Visualization of dystrophic muscle fibers in mdx mouse by vital staining with Evans blue: evidence of apoptosis in dystrophin-deficient muscle. Journal of Biochemistry *118*, 959–964.

Mizushima, N. (2007). Autophagy: process and function. Genes Dev. *21*, 2861–2873.

Monks, J., Rosner, D., Jon Geske, F., Lehman, L., Hanson, L., Neville, M.C., and Fadok, V.A. (2005). Epithelial cells as phagocytes: apoptotic epithelial cells are engulfed by mammary alveolar epithelial cells and repress inflammatory mediator release. Cell Death Differ *12*, 107–114.

Moore, T.Y., Organ, C.L., Edwards, S.V., Biewener, A.A., Tabin, C.J., Jenkins Jr., F.A., and Cooper, K.L. (2015). Multiple Phylogenetically Distinct Events Shaped the Evolution of Limb Skeletal Morphologies Associated with Bipedalism in the Jerboas. Current Biology *25*, 2785–2794.

Moore, T.Y., Rivera, A.M., and Biewener, A.A. (2017). Vertical leaping mechanics of the Lesser Egyptian Jerboa reveal specialization for maneuverability rather than elastic energy storage. Frontiers in Zoology *14*, 32.

Morita, H., Seidman, J., and Seidman, C.E. (2005). Genetic causes of human heart failure. The Journal of Clinical Investigation *115*, 518–526.

Moschella, M.C., and Ontell, M. (1987a). Transient and chronic neonatal denervation of murine muscle: a procedure to modify the phenotypic expression of muscular dystrophy. Journal of Neuroscience *7*, 2145–2152.

Moschella, M.C., and Ontell, M. (1987b). Transient and chronic neonatal denervation of murine muscle: a procedure to modify the phenotypic expression of muscular dystrophy. J. Neurosci. *7*, 2145–2152.

Murphy, M., and Kardon, G. (2011). Origin of vertebrate limb muscle: the role of progenitor and myoblast populations.

Ono, S. (2010). Dynamic regulation of sarcomeric actin filaments in striated muscle. Cytoskeleton (Hoboken, N.J.) *67*, 677–692.

Pavaux, C., and Lignereux, Y. (1995). Une dissection myologique de la Jambe et du Pied de l'Autruche (Struthio camelus)*. Anatomia, Histologia, Embryologia *24*, 127–131.

Pisano, J., Condamine, F.L., Lebedev, V., Bannikova, A., Quere, J.-P., Shenbrot, G.I., Pages, M., and Michaux, J.R. (2015). Out of Himalaya: the impact of past Asian environmental changes on the evolutionary and biogeographical history of Dipodoidea (Rodentia). J. Biogeogr. *42*, 856–870.

Raeker, M.Ö., Shavit, J.A., Dowling, J.J., Michele, D.E., and Russell, M.W. (2014). Membrane-myofibril cross-talk in myofibrillogenesis and in muscular dystrophy pathogenesis: lessons from the zebrafish. Frontiers in Physiology *5*, 14.

Raikow, R.J. (1987). Hindlimb Myology and Evolution of the Old World Suboscine Passerine Birds (Acanthisittidae, Pittidae, Philepittidae, Eurylaimidae). Ornithological Monographs iii–81.

Rhee, D., Sanger, J.M., and Sanger, J.W. (1994). The premyofibril: evidence for its role in myofibrillogenesis. Cell Motility and the Cytoskeleton *28*, 1–24.

Sakuma, K., Aoi, W., and Yamaguchi, A. (2015). Current understanding of sarcopenia: possible candidates modulating muscle mass. Pflügers Archiv - European Journal of Physiology *467*, 213–229.

Sanger, J.M., and Sanger, J.W. (2008). The dynamic Z bands of striated muscle cells. Science Signaling *1*, pe37.

Sanger, J.W., Chowrashi, P., Shaner, N.C., Spalthoff, S., Wang, J., Freeman, N.L., and Sanger, J.M. (2002). Myofibrillogenesis in skeletal muscle cells. Clinical Orthopaedics and Related Research S153-62.

Sanger, J.W., Kang, S., Siebrands, C.C., Freeman, N., Du, A., Wang, J., Stout, A.L., and Sanger, J.M. (2006). How to build a myofibril. Journal of Muscle Research and Cell Motility *26*, 343–354.

Sanger, J.W., Wang, J., Fan, Y., White, J., and Sanger, J.M. (2010). Assembly and dynamics of myofibrils. Journal of Biomedicine & Biotechnology *2010*, 858606.

Schertzer, J.D., Plant, D.R., and Lynch, G.S. (2006). Optimizing Plasmid-Based Gene Transfer for Investigating Skeletal Muscle Structure and Function. Molecular Therapy *13*, 795–803.

Schiaffino, S., Dyar, K.A., Ciciliot, S., Blaauw, B., and Sandri, M. (2013). Mechanisms regulating skeletal muscle growth and atrophy. FEBS Journal *280*, 4294–4314.

Schwegler, M., Wirsing, A.M., Dollinger, A.J., Abendroth, B., Putz, F., Fietkau, R., and Distel, L.V. (2015). Clearance of primary necrotic cells by non-professional phagocytes. Biol. Cell *107*, 372–387.

Souza, M.V., Van Weeren, P.R., Van Schie, H.T.M., and Van De Lest, C.H.A. (2010). Regional differences in biochemical, biomechanical and histomorphological characteristics of the equine suspensory ligament. Equine Veterinary Journal *42*, 611–620.

Stein, B.R. (1990). Limb myology and phylogenetic relationships in the superfamily Dipodoidea (birch mice, jumping mice, and jerboas). Journal of Zoological Systematics and Evolutionary Research *28*, 299–314.

Tidball, J.G., and Wehling-Henricks, M. (2007). Macrophages promote muscle membrane repair and muscle fibre growth and regeneration during modified muscle loading in mice in vivo. The Journal of Physiology *578*, 327–336.

Unguez, G.A., and Zakon, H.H. (1998). Reexpression of myogenic proteins in mature electric organ after removal of neural input. The Journal of Neuroscience : The Official Journal of the Society for Neuroscience *18*, 9924–9935.

Volodin, A., Kosti, I., Goldberg, A.L., and Cohen, S. (2017). Myofibril breakdown during atrophy is a delayed response requiring the transcription factor PAX4 and desmin depolymerization. Proceedings of the National Academy of Sciences *114*, E1375–E1384.

White, R.B., Biérinx, A.-S., Gnocchi, V.F., and Zammit, P.S. (2010). Dynamics of muscle fibre growth during postnatal mouse development. BMC Developmental Biology *10*, 21.

Wortham, R.A. (1948). The development of the muscles and tendons in the lower leg and foot of chick embryos. Journal of Morphology *83*, 105–148.

Wu, C.-L., Cornwell, E.W., Jackman, R.W., and Kandarian, S.C. (2014). NF-κB but not FoxO sites in the MuRF1 promoter are required for transcriptional activation in disuse muscle atrophy. American Journal of Physiology-Cell Physiology *306*, C762–C767.

Wu, S., Wu, W., Zhang, F., Ye, J., Ni, X., Sun, J., Edwards, S.V., Meng, J., and Organ, C.L. (2012). Molecular and Paleontological Evidence for a Post-Cretaceous Origin of Rodents. PLoS ONE *7*, e46445.

Xu, P., Oosterveer, M.H., Stein, S., Demagny, H., Ryu, D., Moullan, N., Wang, X., Can, E., Zamboni, N., Comment, A., et al. (2016). LRH-1-dependent programming of mitochondrial glutamine processing drives liver cancer. Genes & Development *30*, 1255–1260.

Yang, X., Arber, S., William, C., Li, L., Tanabe, Y., Jessell, T.M., Birchmeier, C., and Burden, S.J. (2001). Patterning of muscle acetylcholine receptor gene expression in the absence of motor innervation. Neuron *30*, 399–410.

Supplemental Data

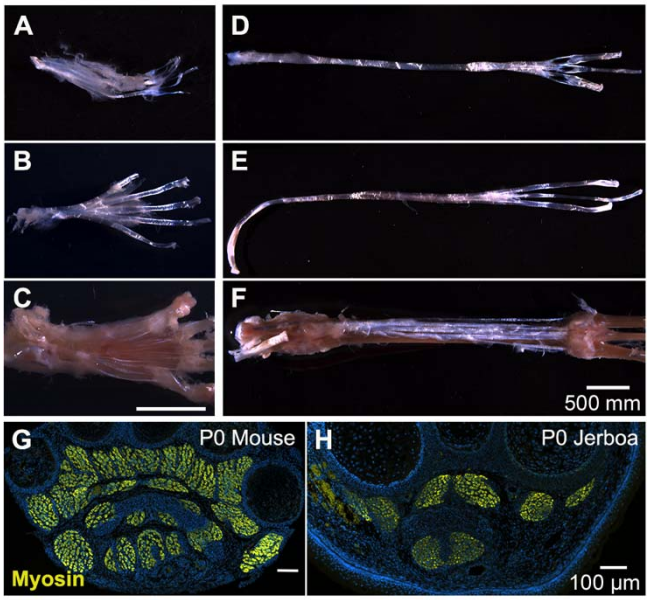

Figure 1 – figure supplement 1. Anatomy of mouse and jerboa foot. Related to Figure 1 and 2. (A) In the adult mouse, tendon of the *flexor digitorum superficialis* supports the *m. flexor digitorum brevis* with distal tendon branches that each divide in two before inserting into either side of the base of the middle phalanx of each digit. (B) Dorsal to this layer, the tendon of the *flexor digitorum longus* splits upon entering the foot and carries the *m. lumbricales.* Each *flexor digitorum longus* tendon emerges distally from between the branches of each *flexor digitorum superficialis* tendon and inserts into the base of each of the terminal phalanges. (C) The *m. interossei* have a common tendon that originates in the tarsus, branches into each of the interosseus muscles, and inserts distally into the base of each of the proximal phalanges. (D-F) The adult jerboa retained the tendons of (D) the *flexor digitorum superficialis*, (E) the *flexor digitorum longus*, and (F) the *interossei*, but all are devoid of muscle. (G, H) A representative transverse section illustrates the presence of foot muscle in the newborn (G) mouse and (H) jerboa.

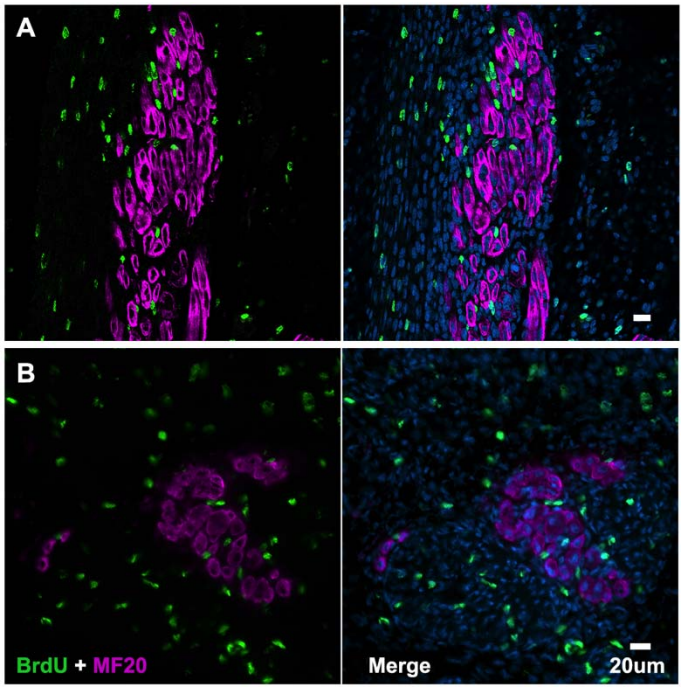

Figure 2 – figure supplement 1. Jerboa foot muscles are postmitotic. Representative image of (A) longitudinal section of P4 (n=1 animal, 156 myofibers) and (B) transverse section of P5 jerboa foot interosseous muscle (n=1 animal, 297 myofibers) illustrating jerboa foot myofibers are postmitotic. BrdU+ nuclei are peripheral to MF20+ myofibers.

Mouse Leg MHC+ nuclei		
	Day 6	Day 9
Litter 1	115	264.5
Litter 2	132.6	128.2
Litter 3	53.6	93.8
Litter 4	98.4	486.8

Mouse Foot MHC+ nuclei		
	Day 6	Day 9
Litter 1	156.8	120
Litter 2	43	129.4
Litter 3	69.4	138.2
Litter 4	294.8	199.4

Jerboa Leg MHC+ nuclei		
	Day 6	Day 9
Litter 1	58.2	74.4
Litter 2	117.5	207.4
Litter 3	100.2	405.8

Jerboa Leg MHC+ nuclei		
	Day 6	Day 9
Litter 1	58.2	74.4
Litter 2	117.5	207.4
Litter 3	100.2	405.8

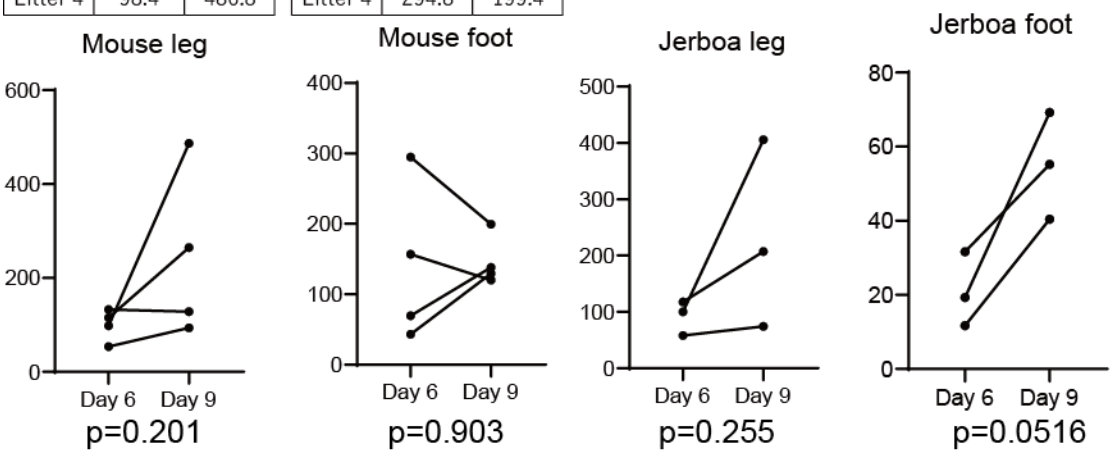

Figure 2 – figure supplement 2. Persistence of differentiated muscle cells in culture after loss *in vivo*. Myoblasts and myocytes were isolated from leg and foot muscles of P1 mouse and jerboa and differentiated in culture for 6 days and 9 days. The number of nuclei within MHC positive cells found in 10 microscopic fields of replica-plated cultures were averaged and represented in graphs and tables. P-values were calculated using paired t-test for replicated wells. None of the experimental groups showed a statistically significant difference in the number of nuclei in Myosin positive cells between Day 6 and Day 9 of culture.

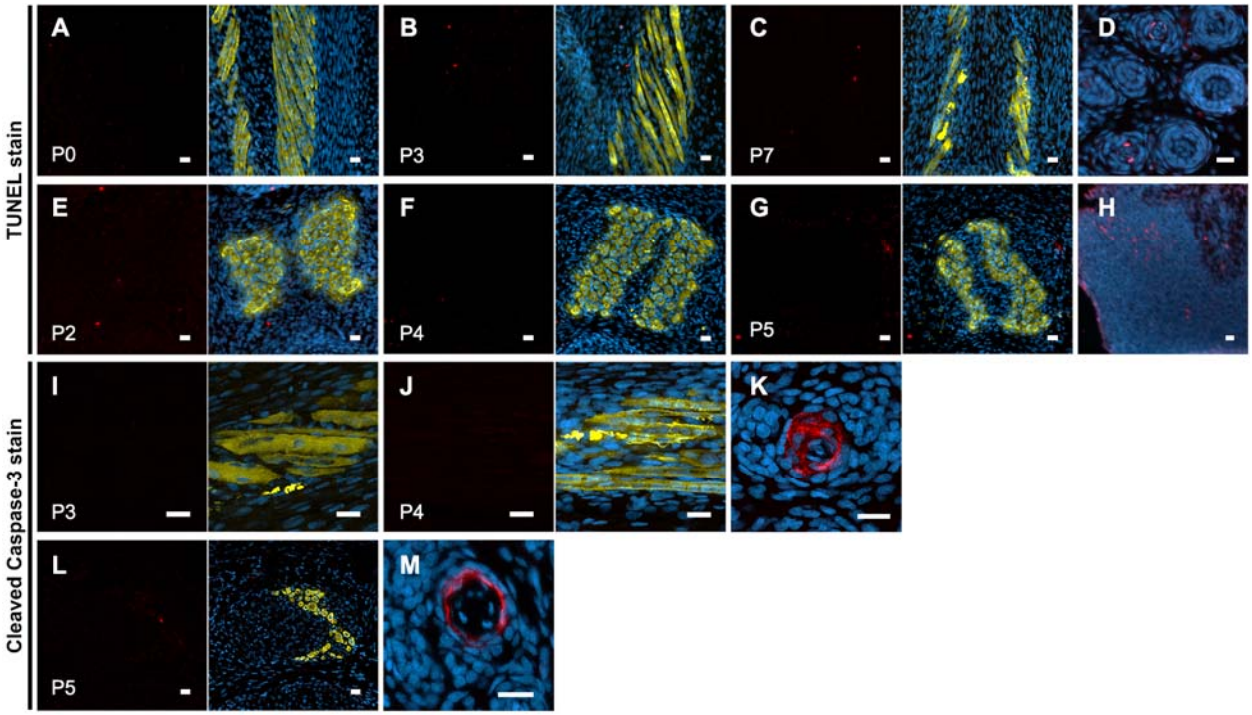

Figure 3 – figure supplement 1. No evidence of jerboa foot muscle apoptosis.
TUNEL staining (TUNEL and merge with DAPI and Myosin) for apoptotic nuclei in longitudinal and transverse sections of interosseous muscle in the (A) P0 (n=1 animal), (B) P3 (n=3), (C) P7 (n=1), (E) P2 (n=2), (F) P4 (n=5), and (G) P5 jerboa foot (n=3). (D) Apoptotic keratinocytes as positive control for A-C and (H) apoptotic limb bud cells as positive control for E-G.
Cleaved Caspase-3 staining (Cleaved Caspase-3 and merge with DAPI and Myosin) for apoptotic nuclei in longitudinal and transverse sections of interosseous muscle in the (I) P3 (n=1 animal), (J) P4 (n=5), (L) P5 jerboa foot (n=2). (K) Apoptotic kerotinocytes as positive control for I-J and in (M) for L. Scale bars are each 20 µm.

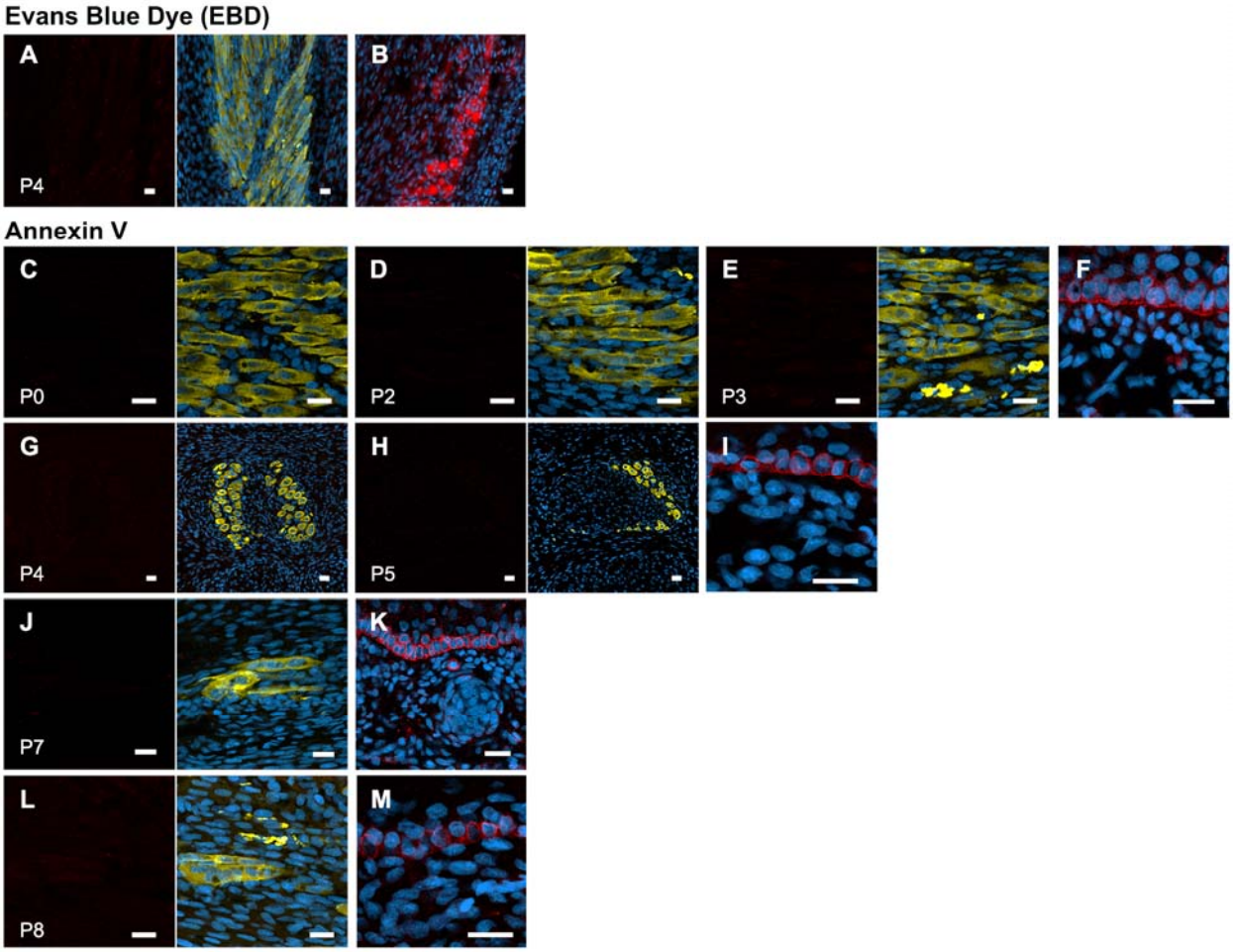

Figure 3 – figure supplement 2. No evidence of jerboa foot muscle necrosis.
(A) EBD detection (EBD and merge with DAPI and Myosin) in longitudinal sections of the third digit interosseous muscle in the P4 jerboa foot (n=5 animals) and of (B) positive control mechanically injured gastrocnemius muscle.
Annexin V immunofluorescence (Annexin V and merge with DAPI annd Myosin) in longitudinal and transverse section of interosseous muscle in the (C) P0 (n=1), (D) P2 (n=1), (E) P3 (n=1), (G) P4 (n=2), (H) P5 (n=1), (J) P7 (n=1), (L) P8 jerboa foot (n=1). (F) Cornifying skin keratinocytes as positive control for C-D, (I) for G-H, (K) for J, and (M) for L. Scale bars are each 20 µm.

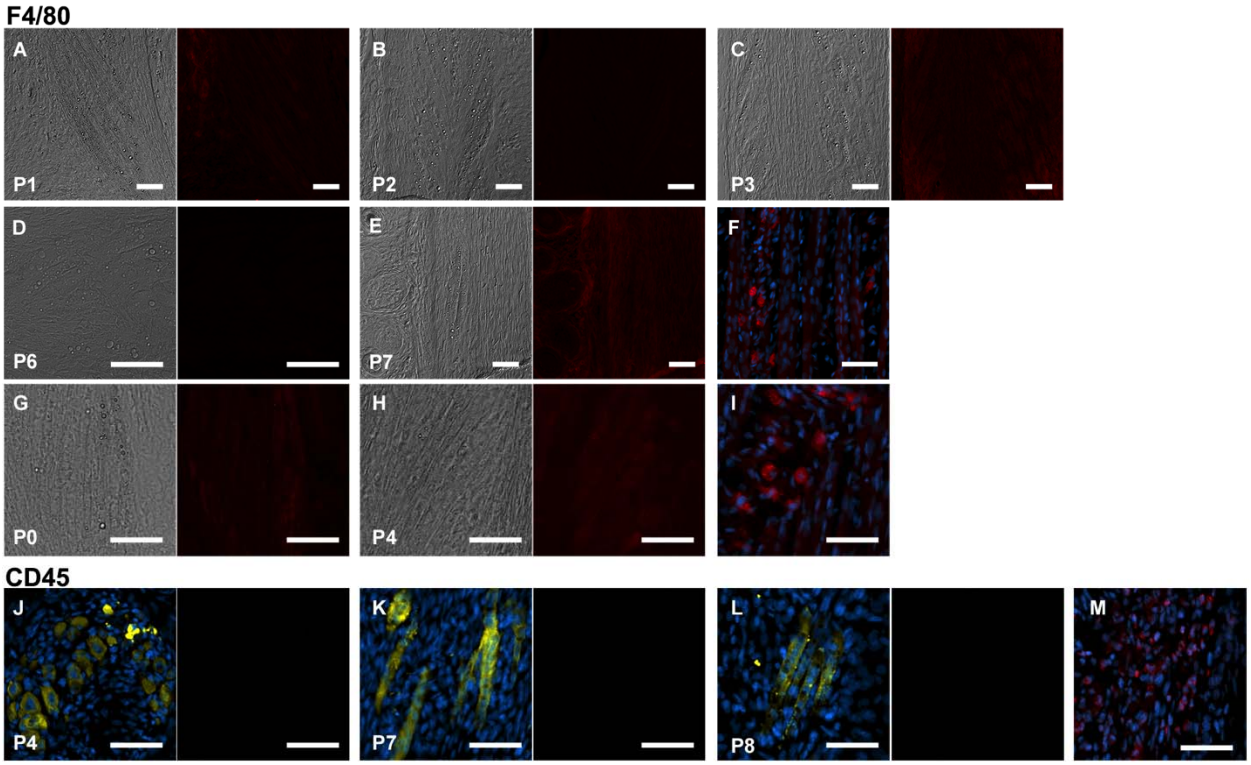

Figure 3 – figure supplement 3. No macrophage infiltration into jerboa foot muscle. Jerboa foot muscles have a distinct morphology and lipid droplets that can be identified by differential interference microscopy in longitudinal sections. F4/80 immunofluorescence in the same longitudinal sections of the third digit interosseous muscle in the (A) P1 (n=2 animals), (B) P2 (n=1), (C) P3 (n=2), (D) P6 (n=2) (E) P7 (n=1), (G) P0 (n=3), and (H) P4 jerboa foot (n=2). Positive control illustrating macrophage presence in mechanically injured jerboa gastrocnemius muscle for A-D in F and for G-H in I.
CD45 immunofluorescence in sections of the third digit interosseous muscle of jerboas. Left panels are a merge of Myosin and DAPI; right panels are CD45 immunofluorescence in (J) P4 (n=3), (K) P7 (n=1), (L) P8 (n=1) animals. Positive control illustrating macrophage presence in mechanically injured jerboa gastrocnemius muscle for J-L in M. Scale bars are each 50 µm.

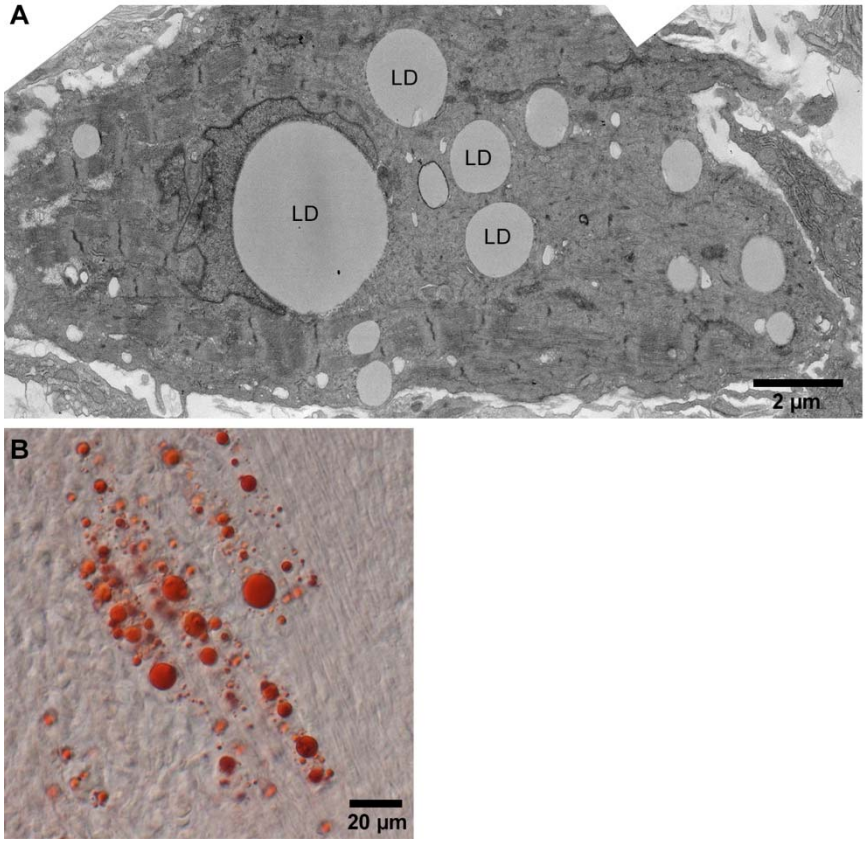

945

Figure 4 – figure supplement 1. Jerboa foot muscle contains large lipid droplets. (A) TEM and (B) Oil red O stained representative images of P4 jerboa foot muscles confirms presence of large lipid droplets. LD in (A) denotes each lipid droplet.

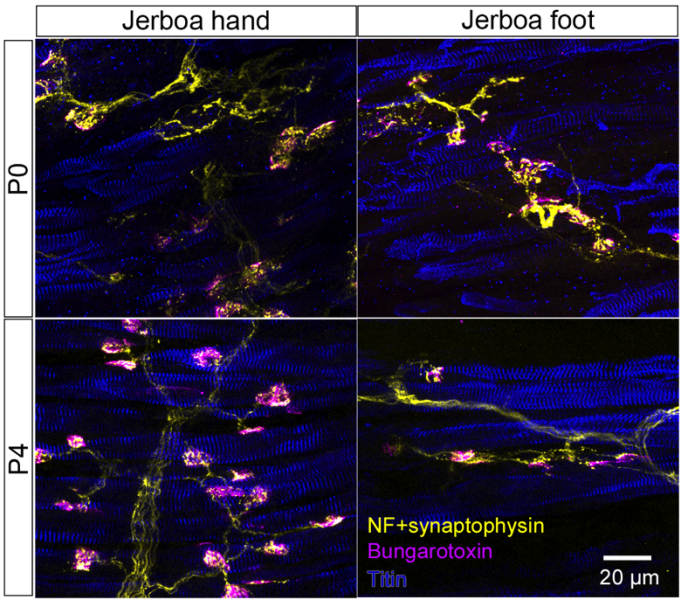

Figure 5 – figure supplement 1. Jerboa foot muscles are innervated.
Representative longitudinal multicolor immunofluorescence images of P0 and P4 jerboa hand and foot muscles with correlated expression of the presynaptic neuronal protein, Synaptophysin, and post-synaptic Acetylcholine Receptor (AchR) (P0: n=4 animals, P4: n=5 animals).

Key			Jerboa foot muscles		
D = Good Desmin			**P0**	**P2**	**P4**
d = Bad Desmin	Group 1	**DRM**	63% ± 26%	23% ± 26%	17% ± 1%
R = Good Tropomyosin		**dRM**	10% ± 2%	5% ± 6%	31% ± 6%
r = Bad Tropomyosin		**Drm**	0	2% ± 3%	0
M = Good Myosin	Group 2a	**rmT**	8% ± 7%	7% ± 7%	23% ± 9%
m = Bad Myosin		**RMt**	1% ± 3%	0	0
T = Good Titin	Group 2b	**RmT**	4% ± 2%	1% ± 3%	17%16%
t = Bad Titin		**rMT**	15% ± 18%	26% ± 11%	12% ± 15%
A = Good α-actinin	Group 3	**mtA**	0	25% ± 21%	25% ± 18%
a = Bad α-actinin		**MTa**	0	0	0
Y = Good Myomesin	Group 4	**mtY**	5% ± 4%	36% ± 18%	27% ± 16%
y = Bad Myomesin		**MTy**	0	0	0

Table S1. Information extracted from multicolor immunofluorescence of individual myofibers to infer the order of sarcomere protein disorganization in jerboa foot muscles. Related to Figure 4. "Good" represents striated localization of each protein to the sarcomere, and "bad" refers to no distinguishable banded pattern of protein expression. In group 1, we saw myofibers with all three proteins properly localized suggesting disorganization follows an initial state of proper localization. When we compared the dRM and Drm categories, we saw loss of Desmin localization when Tropomyosin and Myosin were "good" and almost no myofibers where Desmin was good and the others were bad. This suggests that Desmin is disorganized prior to Tropomyosin and Myosin. In group 2a, there were cells in the rmT category and almost none in the RMt category, suggesting Tropomyosin and Myosin are disorganized prior to Titin. Group 2b illustrates that both categories RmT and rMT appeared at similar frequency, suggesting it is unclear whether Tropomyosin or Myosin become disorganized prior to the other. In group 3, there were cells in the mtA category and none in the MTa category, suggesting Titin becomes disorganized before Alpha-actinin. Similarly, in group 4, there were cells in the mtY category but not in the MTy category suggesting Titin becomes disorganized before Myomesin. Due to shared antibody isotype for Alpha-actinin and Myomesin, the order of disorganization between these two could not be discerned. See Table S2-5 for full details of the percentage of myofibers in each category for each combination of multicolor immunofluorescence.

Key	Stain: Desmin, Tropomyosin, Myosin						
D = Good Desmin		Hand muscles			Foot muscles		
d = Bad Desmin		P0	P2	P4	P0	P2	P4
R = Good Tropomyosin	**DRM**	94% ± 1%	87% ± 2%	96% ± 1%	63% ± 26%	23% ± 26%	17% ± 1%
r = Bad Tropomyosin	**drm**	4% ± 2%	5% ± 7%	0	16% ± 14%	48% ± 15%	36% ± 4%
M = Good Myosin	**dRM**	0	4% ± 5%	4% ± 1%	10% ± 2%	5% ± 6%	31% ± 6%
m = Bad Myosin	**drM**	2% ± 3%	0	0	9% ± 13%	7% ± 10%	7% ± 9%
	dRm	0	4% ± 5%	0	2% ± 0%	6% ± 9%	9% ± 13%
	Drm	0	0	0	0	2% ± 3%	0
	DrM	0	0	0	1% ± 0%	5% ± 6%	0
	DRm	0	0	0	0	5% ± 7%	0
Key	**Stain: Desmin, Myosin, Titin**						
D = Good Desmin		Hand muscles			Foot muscles		
d = Bad Desmin		P0	P2	P4	P0	P2	P4
M = Good Myosin	**DMT**	90% ± 14%	82% ± 13%	95% ± 4%	32% ± 9%	11% ± 15%	7% ± 5%
m = Bad Myosin	**dmt**	0	7% ± 6%	2% ± 3%	26% ± 13%	47% ± 10%	21% ± 23%
T = Good Titin	**dMT**	2% ± 2%	7% ± 4%	3% ± 1%	33% ± 7%	33% ± 23%	33% ± 18%
t = Bad Titin	**dmT**	8% ± 11%	0	0	10% ± 3%	2% ± 3%	38% ± 1%
	dMt	0	0	0	0	6% ± 8%	0
	Dmt	0	0	0	0	0	0
	DmT	0	1% ± 2%	0	0	0	0
	DMt	0	3% ± 4%	0	0	1% ± 2%	0

Table S2. Percentage of myofibers in each category for Desmin, Tropomyosin, Myosin, and Titin multicolor immunofluorescence of jerboa hand and foot muscles at three postnatal stages. Related to Figure 4 and Table S1. For the combination of Desmin, Tropomyosin and Myosin: P0 (2 animals) hand n=78 myofibers and foot n=113 myofibers; P2 (2 animals) hand n=56 and foot n=54 myofibers; P4 (2 animals) hand n=69 and foot n=117 myofibers. For the combination of Desmin, Myosin, and Titin: P0 (2 animals) hand n=48 and foot n=96 myofibers; P2 (2 animals) hand n=71 and foot n=77 myofibers; P4 (2 animals) hand n=63 and foot n=92 myofibers.

Key	Stain: Tropomyosin, Myosin, Titin						
R = Good Tropomyosin		Hand muscles			Foot muscles		
r = Bad Tropomyosin		P0	P2	P4	P0	P2	P4
M = Good Myosin	**RMT**	66% ± 30%	72% ± 25%	91% ± 7%	45% ± 33%	15% ± 21%	24% ± 17%
m = Bad Myosin	**rmt**	6% ± 4%	5% ± 5%	2% ± 4%	18% ± 13%	48% ± 12%	24% ± 5%
T = Good Titin	**rMT**	14% ± 25%	23% ± 27%	3% ± 5%	20% ± 19%	24% ± 11%	12% ± 15%
t = Bad Titin	**rmT**	0	0	0	8% ± 7%	7% ± 7%	23% ± 9%
	rMt	4% ± 5%	0	0	1% ± 2%	5% ± 9%	0
	Rmt	3% ± 2%	0	0	2% ± 4%	0	0
	RmT	5% ± 9%	0	4% ± 4%	3% ± 3%	2% ± 4%	17% ± 16%
	RMt	2% ± 4%	0	0	1% ± 3%	0	0

Table S3. Percentage of myofibers in each category for Tropomyosin, Myosin, and Titin multicolor immunofluorescence of jerboa hand and foot muscles at three postnatal stages. Related to Figure 4 and Table S1. P0 hand (3 animals; n=125 myofibers) and foot (4 animals; n=225 myofibers); P2 (4 animals) hand n=118 and foot n=183 myofibers; P4 (3 animals) hand n=104 and foot n=172 myofibers.

Key	Stain: Myosin, Titin, α-actinin						
M = Good Myosin		Hand muscles			Foot muscles		
m = Bad Myosin		P0	P2	P4	P0	P2	P4
T = Good Titin	**MTA**	76% ± 1%	84% ± 17%	93% ± 6%	55% ± 23%	27% ± 28%	17% ± 3%
t = Bad Titin	**mta**	10% ± 5%	9% ± 13%	2% ± 4%	17% ± 9%	38% ± 32%	34% ± 12%
A = Good α-actinin	**mTA**	12% ± 6%	3% ± 4%	3% ± 3%	12% ± 6%	6% ± 8%	23% ± 15%
a = Bad α-actinin	**mtA**	1% ± 1%	3% ± 3%	2% ± 3%	0	25% ± 21%	25% ± 18%
	mTa	0	0	0	0	0	0
	Mta	0	0	0	0	0	0
	MtA	1% ± 1%	1% ± 2%	0	16% ± 13%	4% ± 3%	1% ± 2%
	MTa	0	0	0	0	0	0

Table S4. Percentage of myofibers in each category for Myosin, Titin, and Alpha-actinin multicolor immunofluorescence of jerboa hand and foot muscles at three postnatal stages. Related to Figure 4 and Table S1. P0 hand (3 animals) n=156 and foot n=182 myofibers; P2 (4 animals) hand n=189 and foot n=203 myofibers; P4 hand (3 animals; n=104 myofibers) and foot (4 animals; n=172 myofibers).

Key	Stain: Myosin, Titin, Myomesin						
M = Good Myosin		Hand muscles			Foot muscles		
m = Bad Myosin		P0	P2	P4	P0	P2	P4
T = Good Titin	**MTY**	100%	82% ± 9%	95% ± 9%	83% ± 7%	29% ± 12%	11% ± 10%
t = Bad Titin	**mty**	0	3% ± 1%	2% ± 4%	3% ± 5%	19% ± 10%	22% ± 9%
Y = Good Myomesin	**mTY**	0	10% ± 12%	2% ± 4%	9% ± 5%	13% ± 19%	24% ± 27%
y = Bad Myomesin	**mtY**	0	3% ± 6%	1% ± 2%	5% ± 4%	36% ± 18%	27% ± 16%
	mTy	0	0	0	0	0	0
	Mty	0	0	0	0	0	0
	MtY	0	1% ± 2%	0	0	4% ± 6%	16% ± 22%
	MTy	0	0	0	0	0	0

Table S5. **Percentage of myofibers in each category for Myosin, Titin, Myomesin multicolor immunofluorescence of jerboa hand and foot muscles at three postnatal stages. Related to Figure 4 and Table S1.** P0 (3 animals) hand n=130 and foot n=159 myofibers; P2 (3 animals) hand n=126 and foot n=142 myofibers; P4 hand (3 animals; n=98 myofibers) and foot (4 animals; n=164 myofibers).